TAMPERE UNIVERSITY OF TECHNOLOGY

ATTE RÄTTYÄ

CFD ANALYSIS OF A HORIZONTAL PULPER

Master of Science Thesis

Examiner: Prof. Reijo Karvinen
Examiner and topic approved by the
Faculty Council of the Faculty
of Engineering Sciences on
14 August 2016

ABSTRACT

ATTE, RÄTTYÄ: CFD Analysis of a Horizontal Pulper
Tampere University of Technology
Master of Science Thesis, 56 pages, 1 Appendix page
October 2016
Master's Degree Programme in Environmental and Energy Technology
Major: Energy efficiency
Supervisors: D.Sc Juha-Pekka Huhtanen, D.Sc Matti Lindstedt
Examiner: Professor Reijo Karvinen

Keywords: Pulper, Paper Pulp, Computational Fluid Dynamics

Pulpers are energy intensive equipment that have been used in paper industry for a long time. Pulper consists of vat and a spinning rotor that mixes the suspension. The energy efficiency and pulping performance of pulpers has improved over the years, but only a few articles have been published on the subject. This is probably due to the fact that pulpers are mainly studied in product development projects.

The objective of this thesis was to perform a series of CFD simulations for a horizontal pulper and evaluate the factors affecting performance of the pulper. Rheological properties of paper pulp were modeled with Herschel-Bulkley material model. Also turbulence was modeled in all simulations. Both stationary and transient simulations were conducted. Fluent 17.0 was used as a solver. Six quantities were defined for pulper performance analysis. These quantities were used to evaluate different pulper configurations. Analysis of the defined quantities yielded extensive data about performance of different rotors and simulation methods. The results were consistent and provided valuable information about flows in the pulper. Also analytical and CFD based sensitivity analysis of the material model was conducted.

Pulper simulation results to this extent have not been published before. Also the quantities defined in this work are published for the first time in a pulper related study. The defined quantities need to be further reviewed. However, the use of these quantities gave promising results in pulper performance analysis. The strengths and weaknesses of different rotors and simulation methods were identified. High pump blades increased rotor efficiency by 3 % when compared to the base case. Also pulping performance was improved. Using completely different rotor geometry increased rotor efficiency over 14 % compared to the base case. More experimental work is needed to verify the results of this study. However, it is difficult and often impossible to measure suspension flows in pulpers. This is why CFD is a valuable tool in pulper design projects.

TIIVISTELMÄ

ATTE, RÄTTYÄ: Vaakapulpperin virtaussimulointi
Tampereen teknillinen yliopisto
Diplomityö, 56 sivua, 1 liitesivu
Lokakuu 2016
Ympäristö- ja energiatekniikan diplomi-insinöörin tutkinto-ohjelma
Pääaine: Energiatehokkuus
Ohjaajat: TkT Juha-Pekka Huhtanen, TkT Matti Lindstedt
Tarkastaja: professori Reijo Karvinen

Avainsanat: pulpperi, sellu, virtaussimulointi

Pulpperit ovat energiaintensiivisiä laitteita, joita on käytetty pitkään paperiteollisuudessa. Pulpperi koostuu ammeesta ja pyörivästä roottorista, joka sekoittaa suspensiota. Pulppereiden energiatehokkuus ja pulpperointiteho on parantunut vuosien varrella, mutta aiheesta on julkaistu vain muutamia artikkeleita. Tämä johtuu todennäköisesti siitä, että pulppreita tutkitaan pääasiassa tuotekehityshankkeiden yhteydessä.

Tämän työn tarkoituksena oli suorittaa vaakapulpperille sarja virtaussimulaatioita ja arvioida niiden perusteella vaakapulpperin toimintaan vaikuttavia tekijöitä. Massan reologiset ominaisuudet mallinnettiin Herschel-Bulkley materiaalimallilla. Myös turbulenssi mallinnettiin kaikissa simuloinneissa. Simulointeja suoritettiin aikariippumattomana ja transienttina. Ratkaisijana käytettiin Fluent 17.0 ohjelmistoa. Työssä määriteltiin kuusi suuretta pulpperin toiminnan analysoimiseksi. Näitä suureita käytettiin eri pulpperikokoonpanojen arvioimiseen. Määritettyjen suureiden analysointi tuotti kattavasti tietoa erilaisten roottoreiden ja simulaatiomenetelmien suorituskyvystä. Tulokset olivat johdonmukaisia ja tuottivat arvokasta tietoa sellun virtauksista pulpperissa. Tämän työn puitteissa suoritettiin myös analyyttinen ja virtaussimulointiin perustuva materiaalimallin herkkyysanalyysi.

Näin kattavia pulpperisimulaatioiden tuloksia ei ole ennen julkaistu. Myös tässä työssä määritellyt suureet julkaistaan nyt ensimmäistä kertaa pulppereihin liittyvän tutkimuksen yhteydessä. Määritettyjä suureita tulee vielä arvioida. Näitä suureita käyttämällä saatiin kuitenkin aikaan lupaavia tuloksia pulpperin suorituskykyä arvioitaessa. Eri roottoreiden ja simulointitapojen vahvuudet ja heikkoudet pystyttiin tunnistamaan. Korkeat pumppusiivet paransivat roottorin hyötysuhdetta 3 % verrattuna lähtötilanteeseen. Myös pulpperointitehokkuus parani. Täysin erilainen roottorigeometria paransi roottorin hyötysuhdetta yli 14 % lähtötilanteeseen verrattuna. Saatujen tulosten varmentamiseksi tulee suorittaa mittauksia. Virtaussuureiden mittaaminen pulpperissa on kuitenkin haastavaa ja usein jopa mahdotonta. Tästä syystä virtaussimulointi on hyödyllinen työkalu pulpperin suunnittelussa.

PREFACE

This thesis was commissioned by Valmet Technologies Inc. during spring 2016. Most of the work was carried out at FS Dynamics Finland office in Tampere. I want to thank Reijo Karvinen for providing the research topic and examining this work. I am also grateful for the knowledge and funding that people from Valmet Technologies decided to contribute to this project. Especially I want to thank Juha-Pekka Huhtanen and Tapio Marjamäki.

I am grateful for the knowledge and support I received from Kati Lindroos, Matti Lindstedt, Arttu Laaksonen and Antti Lehtinen from FS Dynamics Finland during this project. Matti Lindstedt provided many insightful improvements to this thesis.

I want to thank my parents for the substantial support they gave me during my studies. I also want to thank my wife Saara for your support and understanding during this project.

Tampere, 18 October 2016

Atte Rättyä

TABLE OF CONTENTS

LIST OF FIGURES

NOTATIONS

Letter entries

a	Experimental coefficient in yield stress correlation	
A	Area	
b	Experimental coefficient in yield stress correlation	
$C_{1\varepsilon}$	Constant in k-ε model	
$C_{2\varepsilon}$	Constant in k-ε model	
C_m	Mass consistency	
C_μ	Parameter in k- ε turbulence model	
$\underline{\underline{D}}$	Rate of deformation tensor	
$\underline{f}$	Force vector	
g	Gravitational acceleration	
G_k	Rate of production of k due to mean velocity components	
I_S	First invariant of rate of deformation tensor	
II_S,	Second invariant of rate of deformation tensor	
III_S	Third invariant of rate of deformation tensor	
k	Turbulence kinetic energy, consistency index in Herschel-Bulkley material model	
l_m	Mixing length	
L	Length-weighted average fiber length	
m	Fluid consistency index of Power-law model	
n	Flow behaviour index	
$\underline{n}$	Normal vector	
N	Crowding factor	
N_q	Pump specific speed	
p	Pressure	
p_s	Static pressure	Pa
P_{flow}	Power going from rotor to flow	kW
P_{shaft}	Shaft power	kW
Q	Flow rate	m^3/s
$\underline{r}$	Radius vector	
S	Sensitivity	
S_Φ	Generation or destruction of Φ	
t	Time	
u	Velocity in x-direction (or in general)	m/s
u'	Fluctuating velocity component in x-direction	m/s
$\underline{u}_{rad,pos}$	Positive radial velocity vector	m/s
v	Velocity in y-direction	m/s
v'	Fluctuating velocity component in y-direction	m/s
$V_{\Phi,over\ x_1}$	Volume of threshold integral	m^3
w	Velocity in z-direction	m/s
w'	Fluctuating velocity component in z-direction	m/s
x	x coordinate	
y	y coordinate	
Y_k	Dissipation of k due to turbulence	

Y_ω	Dissipation of ω due to turbulence	
z	z coordinate	

Greek letters

Γ	Diffusion coefficient	
Γ_k	Effective diffusivity of k	
Γ_ω	Effective diffusivity of ω	
$\dot{\gamma}$	Shear rate	1/s
$\dot{\gamma}_{\mathrm{c}}$	Critical shear rate	1/s
ε	Turbulence dissipation rate	m^2/s^3
η_{rotor}	Rotor efficiency	
μ	Dynamic viscosity	
μ_{ap}	Apparent molecular dynamic viscosity	Pa·s
μ_{eff}	Effective viscosity	Pa·s
μ_{t}	Turbulent dynamic viscosity	Pa·s
ν_{t}	Turbulent kinematic viscosity	
ρ	Density	kg/m^3
σ_k	Turbulent Prandtl number for k	
σ_ε	Turbulent Prandtl number for ε	
τ	Shear stress	Pa
τ_{c}	Critical shear stress	Pa
τ_{ij}	Shear stresses expressed in Einstein notation	Pa
τ_{xx}	Normal stress in x-direction	Pa
τ_{yy}	Normal stress in y-direction	Pa
τ_{zz}	Normal stress in z-direction	Pa
τ_{y}	Yield stress	Pa
Φ	General property	
Φ_{thr}	Threshold value in volumetric integrals	
ω	Fiber coarseness, rotational speed	rad/s
$\underline{\omega}$	Angular velocity vector	rad/s

Abbreviations

CFD	Computational Fluid Dynamics
DNS	Direct numerical simulation
LES	Large eddy simulation
MRF	Moving Reference Frame
SEC	Specific Energy Consumption

1. INTRODUCTION

Horizontal pulper is used in paper production to slush the paper web during a web break. Reliable operation of horizontal pulper is essential. The faulty web has to be removed from the wire and fed to the pulper at the same rate as the paper machine runs. Pulpers are generally divided to horizontal and vertical pulpers based on the orientation of rotor axel. Horizontal pulpers are used under paper machine because of limited headroom (Paulapuro, 2008, p. 80). Structure of a horizontal pulper is presented in Fig. 1.Vertical pulpers are commonly used for bale and trim pulping. Pulpers have generally been regarded as quite inefficient devices. They use up to 5-15 % of the total energy required in paper production. (Savolainen et al., 1991, p. 147) It is not surprising that ways to decrease pulper's energy consumption have been studied. However, only few studies have been published on the matter.

It is difficult to measure flow velocities or turbulence quantities in a pulper. Wood fiber suspension is opaque and blocks most of the conventional fluid visualization methods. This is why Computational Fluid Dynamics (CFD) simulation of papermaking machines has gained increasing interest (Huhtanen, 2004; Jäsberg, 2007; Hammarström, 2004; Hämäläinen, et al., 2010). Paper pulp is also highly Non-Newtonian. This poses a challenge for both measuring and simulating suspension flow. Also the lack of quantities describing pulping performance poses challenges when new pulpers are developed. There is a great energy saving potential in Pulpers. In the past pulping performance of a pulper could not be evaluated without expensive measurements. In this study a new way to evaluate pulping performance with CFD simulation is proposed.

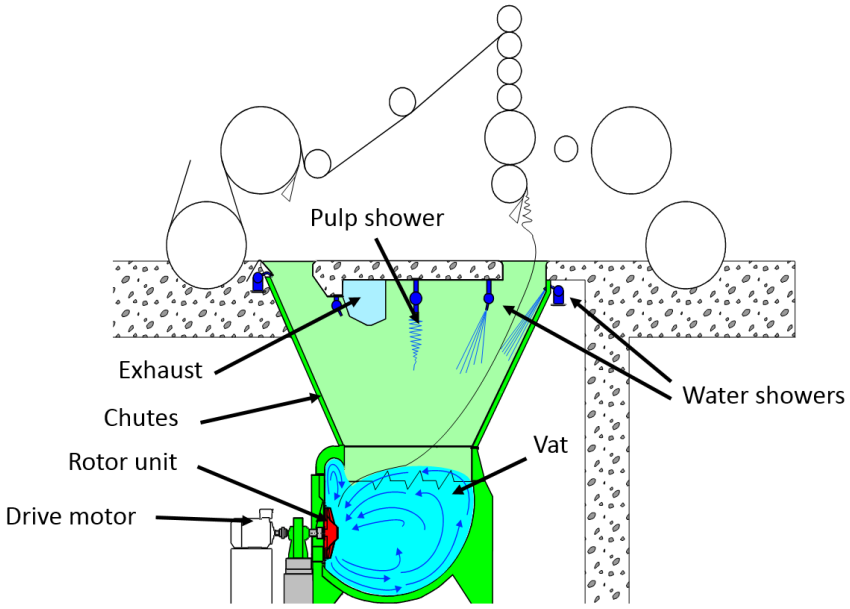

Figure 1. *Structure of a horizontal pulper. (Valmet Technologies Inc., 2015)*

Savolainen et al. (1991) conducted tests on a bale pulper. The tests showed that process temperature, rotor geometry and consistency affect pulping efficiency. Demler and Egan (2004) performed Computational Fluid Dynamics simulations for a vertical pulper. Rotor power in simulations was compared to measured power data. The simulations predicted rotor power with good accuracy. A more energy efficient rotor was developed based on the simulations. The models used in these simulations were quite simple.

The objective of this study was to form a thorough understanding of factors affecting the performance of a horizontal pulper. Low energy consumption cannot be the only goal of pulper development. Pulper's ability to introduce paper web to the suspension and slushing capability are also crucial. This is why the scope of this work is not only energy efficiency, but the overall performance of horizontal pulper.

In this study pulper performance was evaluated using CFD. Herschel-Bulkley material model was used to describe the Non-Newtonian behaviour of paper pulp. Altogether 17 cases were simulated and analyzed. This provided a good understanding of the qualities of different modeling methods and rotor designs. The effects of suspension consistency and material model on simulations were also analyzed. The study showed that rotor efficiency can be increased significantly by changing rotor geometry. Six quantities were defined to analyze pulper performance. These quantities were used to analyze also deflaking characteristics of different rotors. More traditional methods like velocity contours and average velocities were also used to analyze mixing in the pulper.

2. THEORY OF NON-NEWTONIAN FLUIDS

Fluids are divided to Newtonian and non-Newtonian according to their behavior under flow conditions where shear forces occur. In this chapter the fundamental properties of Newtonian and non-Newtonian fluids are presented. Some models to describe non-Newtonian fluid behavior are also discussed.

2.1 Newtonian fluids

An incompressible fluid can be described Newtonian if the behavior obeys the relation expressed in the following Newtonian constitutive equation

$$\underline{\underline{\tau}} = -\mu\underline{\underline{\dot{\gamma}}}\,. \tag{2.1}$$

The Newtonian constitutive equation states how shear stress depends on shear rate and viscosity. In Eq. 2.1 $\underline{\underline{\tau}}$ is shear stress tensor, μ is the Newtonian shear viscosity and $\underline{\underline{\dot{\gamma}}}$ is called shear rate tensor or rate of strain tensor. (Morrison, 2001, pp. 73-75; Chhabra, 2008, pp. 1-2) By definition the Newtonian shear viscosity depends only on material, temperature and pressure, but not shear rate or shear stress (Chhabra, 2008, p. 2). It should be noted that in general the stress tensor can include other than shear stress components (Versteeg, 2007, pp. 21-22; Morrison, 2001, pp. 72-73). In a simple shear flow case all the components of stress tensor are shear stress components and stress tensor is called shear stress tensor. A simple shear flow case is presented in Fig. 2. In the case presented above the upper wall is moving at velocity u to the positive x-direction and the gap is filled with fluid. The movement of upper wall causes a linear velocity profile in fluid. In this simple case shear rate is defined as a velocity gradient.

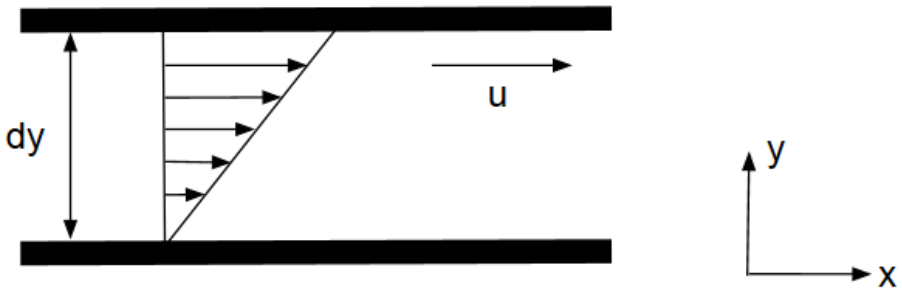

Figure 2. *A Simple shear flow case.*

In this two dimensional case the Eq. 2.1 can be written simply as

$$\tau = -\mu \frac{du}{dy}, \tag{2.2}$$

where u is the velocity in x-direction and dy is the gap height. (Chhabra, 2008, pp. 1-2) In a three dimensional case the shear rate is defined based on rate of deformation tensor. The rate of deformation tensor is defined as

$$\underline{\underline{D}} = \frac{1}{2}\left(\nabla \underline{u} + \left(\nabla \underline{u}\right)^T\right), \tag{2.3}$$

where $\underline{u}$ is the velocity vector in three dimensions (Malvern, 1969, p. 131). Now we can define the three dimensional form of shear rate as follows:

$$\dot{\gamma} = \sqrt{2\underline{\underline{D}} : \underline{\underline{D}}}. \tag{2.4}$$

Eq. 2.4 gives the magnitude of shear rate, which is a scalar. The magnitude of shear rate is defined in a different manner in two dimensional and three dimensional cases. In Fluent 17.0 shear rate is defined in Cartesian coordinate system as (ANSYS, 2015)

$$\dot{\gamma}^2 = 2\left[\left(\frac{\partial u}{\partial x}\right)^2 + \left(\frac{\partial v}{\partial y}\right)^2 + \left(\frac{\partial w}{\partial z}\right)^2\right] + \left(\frac{\partial v}{\partial x} + \frac{\partial u}{\partial y}\right)^2 + \left(\frac{\partial v}{\partial z} + \frac{\partial w}{\partial y}\right)^2 + \left(\frac{\partial w}{\partial x} + \frac{\partial u}{\partial z}\right)^2. \tag{2.5}$$

Shear rate is part of energy dissipation term that describes the dissipation of energy due to viscous forces (Versteeg, 2007, p. 23). In incompressible case viscous dissipation term is defined as shear rate squared times dynamic viscosity.

2.2 Non-Newtonian fluids

The most distinctive difference between Newtonian and Non-Newtonian fluids is that viscosity of a non-Newtonian fluid depends also on other factors than material, temperature and pressure. The viscosity of a non-Newtonian fluid can depend on flow domain geometry, shear stress and even flow history (Chhabra, 2008, p. 5). Non-Newtonian fluids are often split to three categories: Generalized Newtonian fluids, time-dependent fluids and visco-elastic fluids (Chhabra, 2008, p. 5).

A plot of shear stress versus shear rate for a certain fluid is called a flow curve. Flow curves are often used to visualize Non-Newtonian properties of fluids. For a Newtonian fluid the flow curve is a straight line, which crosses the x-axis at the origin. For shear thinning and shear thickening fluids the curve is nonlinear. Flow curves of most common time-independent fluids are presented in Fig. 3.

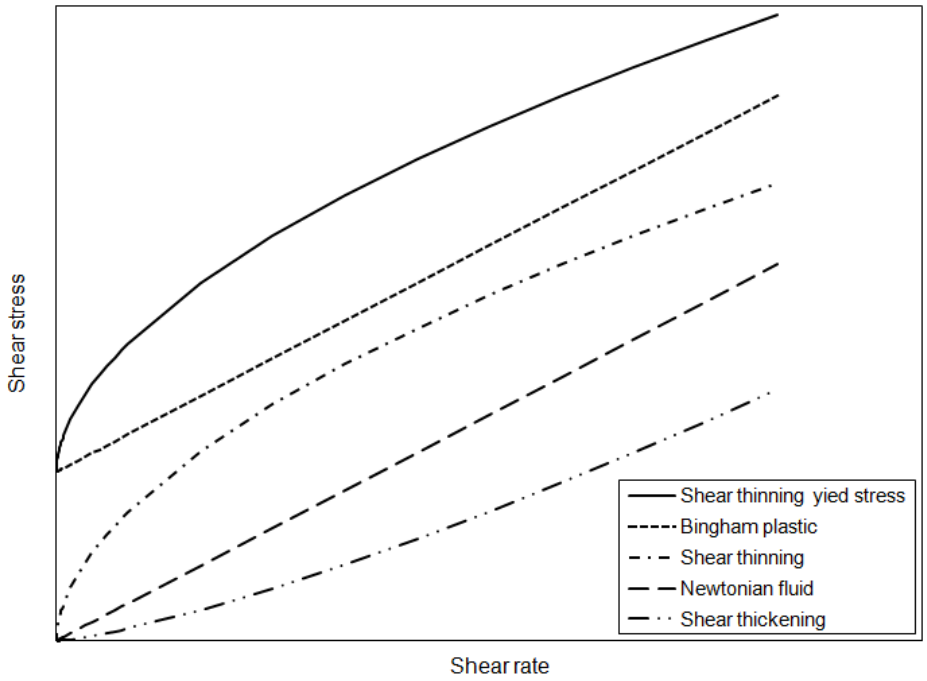

Figure 3. *Flow curves of different time-independent fluids.*

2.2.1 Shear thinning and shear thickening fluids

Non-Newtonian fluids are regarded as shear thinning and shear thickening fluids based on their behavior under shear stress. The viscosity of shear thinning fluid decreases when shear force is applied to the fluid. Correspondingly, the viscosity of shear thickening fluid increases when shear force is applied. Shear thinning and shear thickening fluids are also called pseudoplastic or dilatant, respectively. Ketchup and paint are common shear thinning fluids. Paper pulp is also highly shear thinning. Concentrated suspensions of titanium dioxide and corn flour exhibit shear thickening properties. (Morrison, 2001, pp. 2-7)

Shear thinning is a common time-independent Non-Newtonian effect. Many shear thinning fluids exhibit constant viscosity at very high and very low shear rates. This means that many shear thinning fluids have regions where they behave like Newtonian fluids. The constant viscosity at low shear rates is called zero shear viscosity and the constant viscosity observed at high shear rates is called infinite shear viscosity. Shear thickening fluids can also exhibit irregular behaviour at some shear rates. Some shear thickening fluids even turn to shear thinning at some range of shear rate. Shear thickening fluids are typically concentrated suspensions. According to the current understanding shear thickening results from changes in particle distribution in fluid (Boersma, Laven, Stein, 1992; Hoffman, 1974). (Chhabra, 2008, pp. 12-16)

2.2.2 Yield-stress fluids

Non-Newtonian fluids can also be categorized based on their tendency to start flowing. Some fluids flow only after the stress exceeds certain threshold value. These fluids are called yield-stress fluids or viscoplastic fluids. Yield-stress fluids retain their structure when stress forces are smaller than the yield stress. When stress forces exceed the yield stress value, a yield-stress fluid starts to flow. (Morrison, 2001, pp. 2-7)

A force that does not exceed the yield stress can cause elastic deformation or induce a flow of rigid body of a fluid. Yield stress is caused by rigid structures in the fluid. The structures break when the yield stress is exceeded. In some fluids the particles can't form a rigid structure when it is broken for the first time, or the structure is much weaker than initially. For some fluids, like paper pulp, the yield stress remains approximately the same after first fluidization. The viscosity of a yield-stress fluid can be constant or nonlinear after fluidization. Yield-stress fluids that exhibit constant or nonlinear viscosities are called Bingham plastics and Yield-pseudoplastics, respectively. Many particle suspensions, foodstuffs and drilling muds are yield-stress fluids. (Chhabra, 2008, p. 12)

2.2.3 Time-dependent fluid behaviour

For some fluids the structures in fluid change over time when subjected to constant shear. If shearing breaks down structures the apparent viscosity tends to fall. In some quite rare cases shearing builds up structures in fluid and the viscosity rises. If the apparent viscosity of a fluid under constant shear decreases over time, the fluid is called thixotropic. Correspondingly, if under constant shear the apparent viscosity of a fluid increases over time, the fluid is called rheopectic. Some time-dependent fluids are able to regain their initial viscosity after the shearing has stopped, but the change in viscosity can also be permanent. Some crude oils and foodstuffs are thixotropic. Paper pulp has been found to exhibit thixotropy, but mechanism behind it is not fully understood (Derakhshandeh, 2011, pp. 98-99). Coal-water slurries, protein solutions and gypsum paste are rheopectic fluids. (Chhabra, 2008, pp. 18-21)

2.2.4 Viscosity of Non-Newtonian fluids

Effective dynamic viscosity consists of molecular and turbulent viscosity as follows:

$$\mu_{\text{eff}} = \mu_{\text{t}} + \mu_{\text{ap}} \,, \tag{2.6}$$

where μ_{ap} is apparent molecular dynamic viscosity and μ_{t} is turbulent dynamic viscosity. In laminar flow turbulent viscosity does not exist and effective viscosity equals apparent viscosity. Most flows in industrial processes are turbulent. In simulation software turbulent and molecular viscosities are calculated separately. However, turbulent

viscosity and molecular viscosity can't be treated as two totally unrelated variables. They are always linked through the physics of the simulation. Changes in molecular viscosity affect the values of turbulent viscosity and vice versa.

The turbulent viscosity is calculated as

$$\mu_{\mathrm{t}} = \rho C_{\mu} \frac{k^2}{\varepsilon}, \tag{2.7}$$

where ρ is density, k is the turbulence kinetic energy, ε is turbulence dissipation rate and C_{μ} is a constant or a variable depending on the turbulence model (ANSYS, 2015). In general, the molecular viscosity of Non-Newtonian fluids depends on three invariants of the rate of deformation tensor

$$\mu_{\mathrm{ap}} = \mu_{\mathrm{ap}}(I_S, II_S, III_S)\,. \tag{2.8}$$

For incompressible fluids the first invariant is zero, since $I_S = \mathrm{tr}\left(\underline{\underline{D}}\right) = 0$. The third invariant is zero in two dimensional laminar cases, since $III_S = \det\left(\underline{\underline{D}}\right) = 0$. The third invariant should be taken into account in three dimensional turbulent flows. However, it is a common practice to neglect the effect of the third invariant in simulation software (ANSYS, 2015). If the effect of third invariant is left out, the molecular viscosity depends only on the second invariant. In simulation software the effect of second invariant is taken into account by using shear rate to predict molecular viscosity. The error resulting from the omission of third invariant is evident if the normal rates of deformation have a significant effect on turbulence generation. In pulper simulations the effect of normal rates of deformation on turbulence generation is estimated to be relatively small. The resulting error is not studied in this work. Different apparent viscosity models are discussed in more detail in Section 2.3. (Oliveira, 1998, p. 7)

2.3 Models describing Non-Newtonian flow

Many models have been developed to describe the behaviour of non-Newtonian fluids. In this section few of the most used models are introduced. The most common way to model Non-Newtonian fluids is to construct a model for apparent viscosity. Some models have been developed to model drag reduction via modification of wall functions. To model flows of Non-Newtoninan fluids precisely a set of modified constitutive equations would be needed. However, such a model would be really complicated and compute-intensive. (Oliveira, 1998)

2.3.1 Power-law model

Power-law is a simple viscosity model for non-Newtonian fluids. It is used to model shear thinning and shear thickening effects. The model describes apparent molecular dynamic viscosity with the following equation:

$$\mu_{\mathrm{ap}} = m\dot{\gamma}^{n-1}\,, \tag{2.9}$$

where m is the fluid consistency index of Power-law model and n is flow behaviour index. Both m and n are defined based on experimental data. The exponent of $\dot{\gamma}$ is the slope of $\log(\mu)$ versus $\log(\dot{\gamma})$. When $n > 1$, the fluid is shear thickening and when $n < 1$, the fluid is shear-thinning. At $n = 1$ and $m = \mu$ the model gives Newtonian constitutive equation. Due to the simple approach it has certain drawbacks. Power-law model can describe shear thinning and shear thickening fluids only on limited shear rate range. Thus the values of m and n should be defined not only for each fluid, but also for a set of different shear rates. Power-law also fails to predict viscosities at zero – and infinite shear rate. Despite the obvious weaknesses Power-law is widely used in process engineering. (Morrison, 2001, pp. 229-230; Chhabra, 2008, p. 9)

2.3.2 Bingham plastic model

Bingham plastic model is a simple viscosity model that takes into account the yield stress effect. The model does not include shear thickening or shear thinning effects of the fluid. In one-dimensional case the shear stress is calculated as follows:

$$\tau = \begin{cases} \tau_y + \mu_p\dot{\gamma}\,, & \tau \geq \tau_c \\ \dot{\gamma} = 0\,, & \tau < \tau_c\,, \end{cases} \tag{2.10}$$

where μ_p is the plastic viscosity and τ_y is the yield stress. Apparent viscosity is defined as follows:

$$\begin{aligned} \mu_{ap} &= \mu_p + \frac{\tau_y}{\dot{\gamma}}\,, & \dot{\gamma} &\geq \dot{\gamma}_c \\ \lim_{\dot{\gamma}_c \to \infty} \mu_{ap} &= \infty\,, & \dot{\gamma} &< \dot{\gamma}_c\,, \end{aligned} \tag{2.11}$$

where $\dot{\gamma}_c$ is the critical shear rate. Bingham plastic model states that the fluid is stagnant before the yield stress is reached. This can also be seen from Eq. 2.10. Below the critical shear stress the shear rate is defined as zero. (Chhabra, 2008, p. 13)

2.3.3 Herschel-Bulkley model

Herschel-Bulkley viscosity model can be seen as a combination of Power-law and Bingham plastic viscosity models. It models the yield stress and shear thinning or shear

thickening effects of fluid. In Herschel-Bulkley model the shear stress is defined as follows:

$$\tau = \tau_y + k\dot{\gamma}^n \,, \tag{2.12}$$

where k is consistency index of Herschel-Bulkley model and n is the flow index. The consistency indexes of Power-law model and Herschel-Bulkley model are similar, but the values of these indexes are different. In this simple formulation of Herschel-Bulkley model the value of apparent viscosity rises to infinity at zero shear rate. To avoid infinite viscosity, different formulations for the effective viscosity in Herschel-Bulkley model have been developed (ANSYS, 2015; Chhabra, 2008, p. 14). The model that is used in Fluent 17.0 is written as

$$\mu_{ap} = \begin{cases} \dfrac{\tau_y\left(2 - \dfrac{\dot{\gamma}}{\dot{\gamma}_c}\right)}{\dot{\gamma}_c} + k(\dot{\gamma}_c)^{n-1}\left[(2-n) + (n-1)\dfrac{\dot{\gamma}}{\dot{\gamma}_c}\right], & \dot{\gamma} < \dot{\gamma}_c \\ k\dot{\gamma}^{n-1} + \dfrac{\tau_y}{\dot{\gamma}}, & \dot{\gamma} > \dot{\gamma}_c \end{cases} \tag{2.13}$$

(ANSYS, 2015). Consistency – and flow indexes and yield stress have to be determined experimentally. In Fig. 4 the apparent viscosity and shear stress of a Herschel-Bulkley fluid are plotted against shear rate. Model parameters used in Fig. 4 are: $\dot{\gamma}_c$ = 100 1/s, k = 4.5, n = 0.25 and τ_y = 200 Pa.

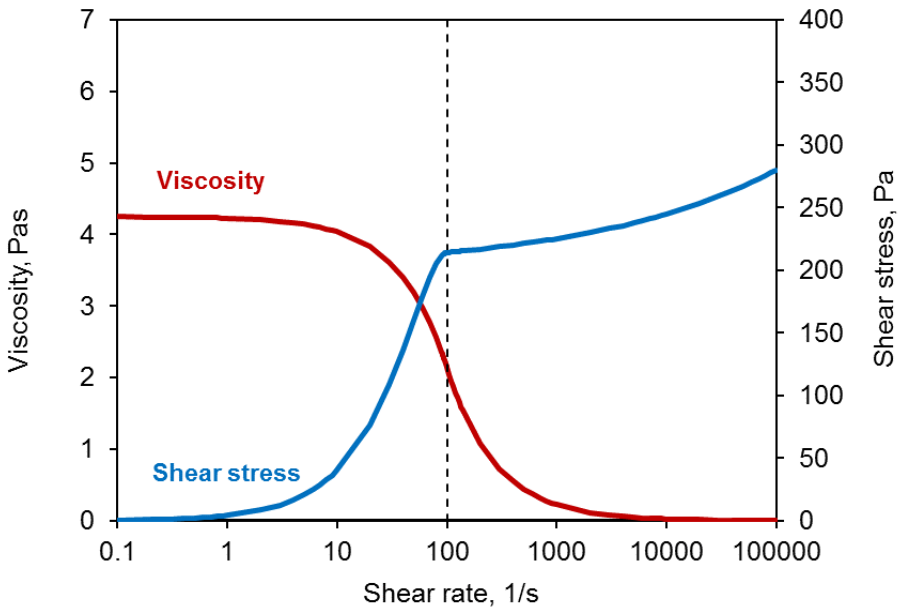

Figure 4. *Shear stress and apparent viscosity in Herschel-Bulkley model.*

2.4 Paper pulp

Paper pulp is a water-fiber suspension that is processed in large quantities in papermaking industry. The knowledge of properties of water-fiber suspensions is important when designing new process equipment for paper industry. Properties of paper pulp change a lot depending on the consistency, freeness, temperature and composition of the pulp. Paper pulp is a heterogeneous mixture of wood fibers and water. Properties of fibers vary considerably even in a pulp made of homogenous tree.

Paper pulp is highly non-Newtonian, thixotropic and shear thinning yield-pseudoplastic fluid. Paper pulp is also opaque even as a relatively dilute solution and exhibits wall slippage in various measurement configurations (Mustalahti, 2015, p. 18; Derakhshandeh, 2011, pp. 61-63). Predicting the flow behaviour of paper pulp is demanding and gaining information of flow patterns is restricted due to the opaque texture of suspension. These properties make paper pulp a challenging material to study. This sets also an evident challenge to designing process equipment for papermaking industry. Despite the challenges of the material a great deal of studies has been published to determine and model the properties of paper pulp (Derakhshandeh et al. 2011; Jäsberg, 2007; Huhtanen, 2004; Bennington & Kerekes, 1996; Hammarström, 2004; Mustalahti, 2015). In this section rheological properties of water-fiber suspensions in papermaking industry are reviewed.

2.4.1 Rheological properties of paper pulp

The rheological properties of paper pulp derive from the properties of wood pulp fibers. Fibers are typically 1-3 mm long and have a diameter of 15-30 μm (Derakhshandeh et al., 2011, p. 3461). Fiber-fiber contacts in water-fiber suspension account for the most rheological properties observed in paper pulp. Fibers have large aspect ratio, which causes large number of contacts between fibers. The probability of fiber-fiber contacts in a suspension is described by a crowding factor

$$N \approx 5.0 C_{\mathrm{m}} \frac{L^2}{\omega}, \tag{2.14}$$

where C_{m} is mass consistency, L is length-weighted average fiber length and ω is fiber coarseness (Kerekes, Schell, 1992). Below $N \approx 16$ the suspension behaves like a dilute solution. Around $N \approx 60$ fibers have on average three contacts per fiber and start to form flocs and fiber networks that have some mechanical strength. The formation of flocs and fiber network is the phenomenon accountable for yield stress in paper pulp.

Dry wood fibers swell in water so a mass based consistency is often used in literature to describe the amount of fibers in pulp suspension. At really high consistencies volume based values are used. Paper pulp is typically categorized as low consistency ($C_{\mathrm{m}} = 0 -$

8%), medium consistency ($C_\mathrm{m} = 8 - 20\%$), high consistency ($C_\mathrm{m} = 20 - 40\%$) and ultra-high consistency ($C_\mathrm{m} > 40\%$) suspension (Derakhshandeh et al., 2011). In this work all suspensions are in low consistency range.

Freeness is a commonly used quantity that describes the characteristics of pulp suspensions. Freeness is measured by draining a pulp sample on a screen (Standard T 227, 1999). Higher draining rate means higher freeness value. Highly beaten pulps have typically a lower freeness values than unbeaten pulps (Hammarström, 2004, p. 59). In many paper pulp measurements the beating of fibers in pumps and mixers changes the properties of pulp over time (Mustalahti, 2015, p. 62). Beating of fibers decreases freeness values in pulp. This poses a challenge for the reproducibility of measurements. Usually decreasing freeness decreases viscosity of suspension, but also opposite behavior has been reported (Chase, Donatelli, Walkinshaw, 1989). In pulp measurements including a pump or a pulper the beating effect cannot be avoided.

2.4.2 Pipe flow

The flow of paper pulp in pipelines is often encountered in papermaking processes and it has been studied in great detail. In paper pulp flow a water layer tends to form near walls. The phenomenon has mostly been studied in pipe flows. Thickness of the lubrication layer is small compared to the diameter of pipe. In a study conducted by Jäsberg (2007, pp. 99-102) the thickness of lubrication layer in a 40 mm pipe was found to be below 0.5 mm. In the simplest model the height of water annulus in a pipe flow depends on slip velocity, wall shear stress and molecular viscosity. Due to these dependencies the height of water annulus also depends on pulp consistency and flow velocity. (Hammarström, 2004, pp. 65-68)

Flow regimes have been identified already by Robertson and Mason (1957). The number of flow regimes depends on the definition. In this work the practice of five flow regimes presented by Jäsberg (2007) is presented in more detail. The flow regimes presented by Jäsberg (2007) are a slightly modified version of a partition presented by Duffy (1997). The first flow regime is called plug flow with wall contact. In this regime the flow velocity is low and the fibers spread to the whole cross-section of the pipe forming a “plug”. The mechanical contact between fibers and pipe cause high pressure loss per pipe length. If the pressure gradient driving the flow is not high enough to move fiber network, then the carrier fluid flows through stagnant fiber network. This is not considered a flow regime, since the fibers in suspension do not move with the flow. The second flow regime is called plug flow with lubrication layer. When flow velocity is increased inertial lift force moves the fibers away from pipe walls creating a water annulus in pipe. Lubrication layer reduces wall drag and thus the pressure drop stays the same or might even decrease with increasing flow velocity.

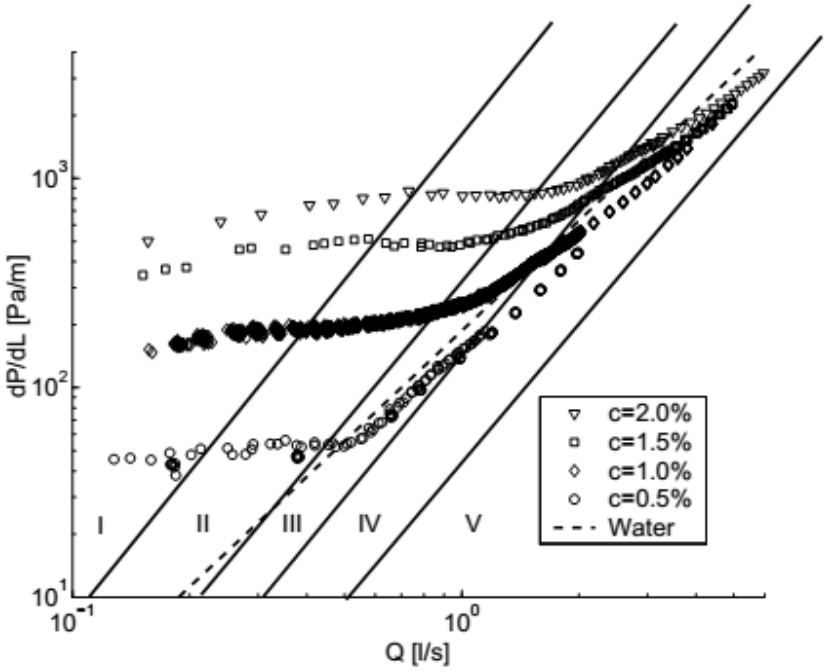

Figure 5. *Flow regimes of pipe flow and pressure loss data for different pulp concentrations. (Jäsberg, 2007, p. 104)*

Third flow regime is called plug flow with smearing annulus. Turbulent fluctuations start to form in water annulus in this flow regime. Pressure drop is increased approximately linearly with increasing flow velocity. Fourth regime is called mixed flow. In this flow regime high flow velocity creates fully turbulent regime in the water annulus. Wall friction and turbulence keep the fibers away from pipe wall. Growth of pressure drop is approximately quadratic with increasing flow velocity. Frictional losses of flow fall below the losses of carrier fluid in third or fourth flow regime. The last flow regime is fully turbulent. Turbulent fluctuations disperse the fiber plug and the fluid becomes gradually homogeneous in terms of fiber concentration. Loss typically approaches the pure carrier fluid loss curve. In Fig. 5 the flow regimes are visualized with pressure loss data.

2.4.3 Yield stress

Yield stress or apparent yield stress is the amount of shear stress that is needed to break a fiber network and induce flow in paper pulp. There are different ways to define yield stress and also various methods to measure it. Three widely used methods to define yield stress are Maximum Viscosity, Apparent stress to initiate flow and Ultimate Shear Strength methods. As yield stress is increased, the instantaneous viscosity of paper pulp first increases and reaches the maximum viscosity. When yield stress is increased after maximum viscosity value the instantaneous viscosity drops. In maximum viscosity method, the yield stress at maximum viscosity is the yield stress. In Apparent stress to initiate flow method, yield stress is defined as shear stress at zero shear rate. Shear stress

is first measured and plotted against shear rate. This plot usually includes a linear part that can be extrapolated to zero shear rate. In Ultimate Shear Strength method strain is increased until stress starts to decrease. In this method the maximum stress during this ramp is the yield stress. Also oscillatory rheometres have been used to measure yield stress of paper pulp (Swerin, et al., 1992). Oscillatory rheometers are potentially accurate in material property measurements, but it is challenging to maintain constant fiber concentration in the rheometer during measurements. (Derakhshandeh , 2011, pp. 5-7)

For paper pulp, a quasi-static and dynamic network strength methods are the most widely used methods to measure yield stress values. Dynamic methods typically result in lower yield stress values than quasi-static methods. Shear levels in fiber suspensions are very difficult to quantify and there are many factors that contribute to yield stress measurement results. This is why there is a significant deviation in yield stress measurements from different experiments. For example, for a 3 % suspension the yield stress values from different studies have ranged from 19,3 Pa to around 300 Pa (Swerin et al., 1992; Ein-Mozaffari et al., 2005). The results of yield stress measurements for pulp concentrations of 3 % and above are usually fitted to the following correlation:

$$\tau_y = a{C_m}^b \,, \tag{2.15}$$

where a and b are experimentally defined coefficients. Experimentally defined values of a and b vary significantly between different studies. (Derakhshandeh, 2011, pp. 7-13)

3. THEORY OF COMPUTATIONAL FLUID DYNAMICS

In computational fluid dynamics or CFD governing equations describing fluid flow are solved numerically using computers. The fundamental equations in fluid dynamics are momentum conservation equations, or Navier-Stokes equations and mass conservation equations. In case energy transfer is examined also energy equations are included. Mass conservation equation can be written in compact vector form as follows:

$$\frac{\partial \rho}{\partial t} + \nabla \cdot (\rho u_i) = 0 \,, \tag{3.1}$$

where ρ is viscosity and u_i is general velocity vector expressed using Einstein notation (Versteeg, 2007, p. 11). In the previous form it is assumed that there are no mass sources. For incompressible flows mass conservation equation can be further simplified

$$\nabla \cdot u_i = 0 \,, \tag{3.2}$$

and Navier-Stokes equation can be written as

$$\rho \left(\frac{\partial u_i}{\partial t} + u_i \cdot \nabla u_i \right) = -\nabla p - \nabla \underline{\underline{\tau}} + \rho \underline{g} \,, \tag{3.3}$$

where p is pressure, $\underline{\underline{\tau}}$ is stress tensor and $\underline{g}$ is the gravitational acceleration vector. (Morrison, 2001, p. 76)

3.1 Turbulence modeling

In general, turbulence is random and three dimensional phenomena. The smallest scales of turbulent motions are typically around 0,1 to 0,01 mm (Versteeg, 2007, p. 42). In small length scale the frequency of motion is high. Thus accurate turbulence simulation requires small mesh elements and time steps. This leads to really high computational costs for simulations. This is why in most CFD simulations turbulence models are used. In Direct Numerical Simulation or DNS turbulence model is not used and the mesh is refined to the level where the smallest scales of turbulence can be calculated. Large Eddy Simulation (LES) distinguishes large eddies from small eddies. The large eddies are simulated in detail whereas small eddies are modeled using a sub-grid scale model. LES requires less computational resources than DNS. In spite of this, LES is rarely used in simulations including complex geometries. The computational resources needed for LES

are significantly greater than with turbulence models for RANS equations. (Versteeg, 2007, pp. 65-67)

Most turbulence models are made for RANS or Reynolds-averaged Navier-Stokes equations. RANS equations are time averaged equations with Reynolds decomposition. RANS equations are used to describe mean flow parameters and the interaction of mean flow and turbulence. For a general property Φ the Reynolds decomposition yields:

$$\Phi = \bar{\Phi} + \Phi' \,, \tag{3.4}$$

where $\bar{\Phi}$ is the mean and Φ' the fluctuating component (Versteeg, 2007, pp. 62-63). For general velocity component u_i Reynolds decomposition gives:

$$u_i = \bar{u}_i + u_i' \,. \tag{3.5}$$

The time averaging operator in Reynolds decomposition is defined as (Versteeg, 2007, p. 50)

$$\bar{\Phi} = \frac{1}{\Delta t}\int_0^{\Delta t} \Phi(t)\, dt \,. \tag{3.6}$$

Reynolds equations for incompressible flow are defined as follows (Versteeg, 2007, pp. 63-64).

$$\frac{\partial \bar{u}}{\partial t} + \nabla \cdot (\bar{u}\bar{u}_i) = -\frac{1}{\rho}\frac{\partial \bar{P}}{\partial x} + \nu \nabla \cdot (\nabla \bar{\mathrm{u}}) + \left[-\frac{\partial \left(\overline{u'^2}\right)}{\partial x} - \frac{\partial \left(\overline{u'v'}\right)}{\partial y} - \frac{\partial \left(\overline{u'w'}\right)}{\partial z} \right] \tag{3.7}$$

$$\frac{\partial \bar{v}}{\partial t} + \nabla \cdot (\bar{v}\bar{u}_i) = -\frac{1}{\rho}\frac{\partial \bar{P}}{\partial y} + \nu \nabla \cdot (\nabla \bar{\mathrm{v}}) + \left[-\frac{\partial \left(\overline{u'v'}\right)}{\partial x} - \frac{\partial \left(\overline{v'^2}\right)}{\partial y} - \frac{\partial \left(\overline{v'w'}\right)}{\partial z} \right] \tag{3.8}$$

$$\frac{\partial \bar{w}}{\partial t} + \nabla \cdot (\bar{w}\bar{u}_i) = -\frac{1}{\rho}\frac{\partial \bar{P}}{\partial z} + \nu \nabla \cdot (\nabla \bar{\mathrm{w}}) + \left[-\frac{\partial \left(\overline{u'w'}\right)}{\partial x} - \frac{\partial \left(\overline{v'w'}\right)}{\partial y} - \frac{\partial \left(\overline{w'^2}\right)}{\partial z} \right] \tag{3.9}$$

For flow simulations the continuity equation and Reynolds equations need to be solved.

3.2 Turbulence models for RANS equations

When Navier-Stokes equation is decomposed and time averaged six extra terms are formed. Three of these terms are normal stresses

$$\tau_{xx} = -\rho\overline{\grave{u}^2} \qquad \tau_{yy} = -\rho\overline{\grave{v}^2} \qquad \tau_{zz} = -\rho\overline{\grave{w}^2} \tag{3.10}$$

and rest of the terms are shear stresses

$$\tau_{xy} = \tau_{yx} = -\rho\overline{\grave{u}\grave{v}} \qquad \tau_{xz} = \tau_{zx} = -\rho\overline{\grave{u}\grave{w}} \qquad \tau_{yz} = \tau_{zy} = -\rho\overline{\grave{u}\grave{w}}\,. \tag{3.11}$$

These terms are called Reynolds stresses (Versteeg, 2007, p. 64). Turbulence models for RANS equations model the impact of these terms on average flow. Turbulence models are categorized according to the number of extra transport equations needed in the model. Mixing length model is the simplest turbulence model, since it has no extra transport equations. Spalart-Allmaras is a simple model with one extra equation. k-ε, k-ω and Algebraic stress model include two extra equations. Reynolds Stress Equation Model or RSM is the most complex turbulence model with seven extra transport equations. Mixing length –, k-ε –, k-ω and Reynolds stress equation models are presented here in more detail.

3.2.1 Mixing length model

In mixing length model and k-ε model an analogy is assumed between the way viscous stresses and Reynolds stresses affect the main flow. In Prandtl's mixing length model turbulent viscosity depends on mixing length and velocity gradient. Reynolds stress is also modeled with mixing length and a velocity gradient. The mixing length depends on flow conditions and geometry. This is why mixing length model can't be used as a universal turbulence model. In free shear flows mixing length depends on the thickness of the shear layer. Prandtl's mixing length model can be expressed as follows:

$$\nu_t = {l_m}^2 \left|\frac{\partial \mathrm{u}}{\partial \mathrm{y}}\right|, \tag{3.12}$$

where ν_t is kinematic turbulent viscosity and l_m is the mixing length (Versteeg, 2007, p. 70). Mixing length model includes also a model for scalar transport. Due to the simplistic nature of mixing length model it is capable of modeling only simple two-dimensional flows with no separation or recirculation. However, it performs well in predicting thin shear layers and simulation run times are low. Mixing length model is used in some more advanced turbulence models in wall boundary condition treatment. (Versteeg, 2007, pp. 69-72)

3.2.2 k-ε model

k-ε model uses transport equations for turbulence kinetic energy and turbulence dissipation rate to simulate turbulence. It is a well established semi-empirical model that

is used widely in industrial simulations. In standard k-ε model the transport equation for turbulence kinetic energy can be written as follows:

$$\frac{\partial(\rho k)}{\partial t} + \frac{\partial(\rho k u_i)}{\partial x_i} = \frac{\partial}{\partial x_j}\left[\left(\mu + \frac{\mu_t}{\sigma_k}\right)\frac{\partial k}{\partial x_j}\right] + G_k - \rho\varepsilon \,, \tag{3.13}$$

where k is the turbulence kinetic energy, σ_k is the turbulent Prandtl number for k and G_k is the rate of production of k due to the mean velocity components (ANSYS, 2015). The transport equation for turbulence dissipation is written as

$$\frac{\partial(\rho\varepsilon)}{\partial t} + \frac{\partial(\rho\varepsilon u_i)}{\partial x_i} = \frac{\partial}{\partial x_j}\left[\left(\mu + \frac{\mu_t}{\sigma_\varepsilon}\right)\frac{\partial \varepsilon}{\partial x_j}\right] + C_{1\varepsilon}\frac{\varepsilon}{k}G_k - C_{2\varepsilon}\rho\frac{\varepsilon^2}{k}, \tag{3.14}$$

where $C_{1\varepsilon}$ and $C_{2\varepsilon}$ are constants and σ_ε is the turbulent Prandtl number for ε (ANSYS, 2015). Standard k-ε model is valid for only fully turbulent flows and it performs poorly in rotating flows and some unconfined flows. There are many variants of k-ε model that seek to improve its performance. RNG and realizable k-ε models are the most used versions. RNG k-ε model performs better with rapidly strained flows, swirly flows and it has a build in model to enhance the treatment of low-Reynolds number flows. Realizable k-ε model has many of the same advantages as RNG version and it performs even better in some cases. Realizable k-ε model is relatively new turbulence model and the benefits and drawbacks associated to it are not yet fully known. It is, however, a very promising turbulence model for many industrial applications. (ANSYS, 2015)

3.2.3 k-ω model

k-ω model is an empirical model that uses specific dissipation rate $\omega = \varepsilon/k$ instead of ε to determine a length scale (Versteeg, 2007, p. 90). In standard k-ω model, introduced by Wilcox (1993), no wall-damping functions are needed in low-Reynolds number flows. On the downside, the solution is sensitive to the values of k and ω outside shear layer. Transport equation for k in k-ω model is written as follows:

$$\frac{\partial(\rho k)}{\partial t} + \frac{\partial(\rho k u_i)}{\partial x_i} = \frac{\partial}{\partial x_j}\left(\Gamma_k \frac{\partial k}{\partial x_j}\right) + G_k - Y_k \,, \tag{3.15}$$

where Γ_k is the effective diffusivity of k and Y_k is the dissipation of k due to turbulence (ANSYS, 2015). The corresponding transport equation for ω is written as

$$\frac{\partial(\rho\omega)}{\partial t} + \frac{\partial(\rho\omega u_i)}{\partial x_i} = \frac{\partial}{\partial x_j}\left(\Gamma_\omega \frac{\partial \omega}{\partial x_j}\right) + G_\omega - Y_\omega \,, \tag{3.16}$$

where ω is the specific dissipation rate, Γ_ω is the effective diffusivity of ω and Y_ω is the dissipation of ω due to turbulence (ANSYS, 2015). Also, k-ω model has been modified

to improve its performance. Most used variations are Baseline (BSL) k-ω model and Shear-Stress Transport (SST) k-ω model. BSL k-ω model exploits the robust features of k-ε model in far field simulation to improve performance outside shear layer. k-ω SST includes the improvements of BSL version and it also takes transport of the turbulence shear stress into account when calculating turbulent viscosity. SST version outperforms BSL in many cases like adverse pressure gradient flows and flows around airflows.

3.2.4 Reynolds Stress Equation Model

Turbulence models with one or two extra equations fail to predict individual Reynolds stresses in complex strain fields. This poses challenges for example in cyclone and rotating flow passage simulations (ANSYS, 2015). RSM has extra transport equations for Reynolds stresses. Thus it can simulate directional effects of Reynolds stresses unlike other RANS turbulence models. With RSM even complex strain fields can be simulate with good accuracy. Reynolds stress transport equation in RSM is defined as

$$\frac{DR_{ij}}{Dt} = \frac{\partial R_{ij}}{\partial t} + C_{\mathrm{ij}} = P_{\mathrm{ij}} + D_{\mathrm{ij}} - \varepsilon_{ij} + \Pi_{ij} + \Omega_{ij}\,, \tag{3.17}$$

where $R_{ij} = \overline{\grave{u}_\iota \grave{v}_j}$ is the Reynolds stress, C_{ij} is transport of R_{ij} by convection, P_{ij} is rate of production of R_{ij}, D_{ij} is transport of R_{ij} by diffusion, ε_{ij} is rate of dissipation of R_{ij}, Π_{ij} is transport of R_{ij} due to turbulent pressure-strain interactions and Ω_{ij} is a rotation term (Versteeg, 2007, p. 81). RSM uses either ω or ε based scale equations (ANSYS, 2015). This means that RSM includes the same scale related assumptions and drawbacks as k-ω or k-ε models, depending on the scale equation. However, it is potentially the most universal classical turbulence model. RSM is computationally intensive due to seven extra partial differential equations. Using RSM instead of a simple turbulence model is not always worth the extra cost. This is why RSM has not been used and validated as extensively as k-ω and k-ε models. (Versteeg, 2007, pp. 80-84)

3.3 Discretization of convection and diffusion

In most fluid flow dominant problems convection has to be taken into account. Convection transfers properties on the flow direction whereas diffusion transfers properties in every direction. Diffusion and convection always occur side by side. Thus it is reasonable to discretize convection and diffusion simultaneously. In steady state, transport equation for convection and diffusion can be written for general property Φ as

$$\nabla \cdot (\rho u \Phi) = \nabla \cdot (\Gamma \nabla \Phi) + S_\Phi\,, \tag{3.18}$$

where Γ is the diffusion coefficient and S_Φ is the generation or destruction of the general property Φ. This equation can be discretized with plenty of numerical methods. Most

important characteristic properties of discretized equations are boundedness, transportiveness, conservativeness and accuracy. Boundedness is composed of two essential criteria. In case there are no sources the values of Φ should be bounded by boundary values. The other criterion states that all coefficients in the discretized equations need to have same sign. Conservativeness is a property that is achieved by matching fluxes of general property Φ in adjacent cells. Transportiveness is a property that is achieved when direction of flow and the magnitudes of diffusion and convection respect to each other are taken into account when calculating the values of Φ. In case these criteria are not met it is possible that the calculation does not converge or the solution fluctuates. (Versteeg, 2007)

Accuracy of differencing schemes is described in terms of Taylor series truncation error. Some of first order differencing schemes are robust, but they often cause numerical diffusion. To achieve all wanted properties in differencing schemes higher order difference schemes are introduced. The QUICK scheme is the oldest higher-order differencing scheme. QUICK uses three-point iteration that is upstream-weighted. QUICK is of third-order in terms of accuracy, it is conservative and it achieves transportiveness. However, it is only conditionally stable due lack of boundedness in some cases. This has been addressed in later variations of the algorithm.

3.4 Pressure-velocity coupling

Pressure-velocity coupling can be done in segregated or coupled manner. In segregated methods the solving procedure is implemented roughly as follows. Initial velocity field is guessed and the continuity equation is solved to obtain pressure correction. Pressures and velocities are corrected and the transport equations for scalar quantities are solved. This procedure is repeated until convergence is achieved. SIMPLE, SIMPLEC and PISO are examples of segregated algorithms. These algorithms solve momentum equation and pressure correction equations separately. In coupled method these equations are solved together.

SIMPLE is usually the standard algorithm for pressure-velocity coupling, but using SIMPLEC can improve convergence in simple laminar flows and in more complex cases if convergence is limited due to pressure-velocity coupling. PISO performs better than SIMPLE or SIMPLEC in transient simulations, especially with large time step. Coupled solution method performs better than segregated algorithms in many steady-state simulations and transient simulations with large time steps or poor mesh quality. (Versteeg, 2007, pp. 186-196)

3.5 CFD simulation of paper pulp

In CFD simulations the desired level of accuracy determines the complexity of used models. Complex models usually lead to computationally intensive simulations. This is also true in paper pulp CFD simulations. Even a simple simulation can give good results if only mean flow parameters are needed (Demler & Egan, 2004). If lubrication layer and the associated drag reduction phenomenon have to be modeled accurately a more elaborate wall slip model is needed (Cotas, Asendrych, Garcia, Faia, & Rasteiro, 2015; Hammarström, 2004, Appendix II). Because of the complexity of the area it is crucial to define the wanted level of accuracy and detail in simulation. Unnecessarily accurate simulation leads to high computational costs.

Simulations where paper pulp is the flowing fluid can be roughly divided to two categories (Cotas, Asendrych, & Rasteiro, 2015, p. 443). In the first category belong the simulations where pulp is modeled as homogenous material. In the simplest simulations pulp is modeled as water and no elaborate model details are involved. These simulations can yield satisfactory results and achieve reasonable agreement with measurements in some cases (Demler & Egan, 2004). This is probably due to the fact that pulp suspension behaves like water in some cases even though the behaviour is different on phenomenal level (Hammarström, 2004, pp. 47-48). In more elaborate simulations in this category generalized Newtonian models are used as a material model. Also custom wall slip functions can be used to model drag reduction. These models offer reasonable accuracy in many cases (Huhtanen, 2004, pp. 85-98; Cotas, Asendrych, Garcia, et al., 2015). However, even a Herschel-Bulkley model that is adjusted based on measurements can yield significant errors if the simulation is not set up correctly or there are uncertainties in measurements (Mustalahti, 2015, pp. 61-63).

The second category consists of simulations where multiphase flow models are used. These models are used regularly in certain cases, but can’t be considered as universal models. Multiphase models have to be used if phase separation needs to be simulated. Even models where individual fibers are simulated have been tested, but they are generally too complex for practical use. Advanced suspension models in papermaking are reviewed by Hämäläinen et al. (2010).

In this work Herschel-Bulkley model is used as a material model. Thus the scope of this work falls in the first simulation category. Simulations in this category have some special traits. In pulp flows with a viscosity model shear rate has a significant effect on the fluid viscosity. Thus turbulence models affect the simulation mainly on regions where shear rate is high and viscosity low. It is likely that only part of the flow field is turbulent. The use of material model should also be considered when constructing the computational mesh. Refining the mesh near walls can have an effect on the velocity gradients near the wall. This leads to altered shear rates and different viscosities. It is clear that mesh

independence should be studied when accurate near-wall treatment is desired (Hammarström, 2004, pp. 55-56).

4. HORIZONTAL PULPER

Horizontal pulper is a part of paper machines broke handling system. The main function of broke system is to repulp broke to a pumpable slurry in case of a web break. This is essential because of two reasons. First, we have to get the faulty web off the wire in a controlled manner. Secondly, it is advisable to reuse all fibers going to the broke. Horizontal pulper is also used to slush trims from wire, winders and sometimes also from reel slab-offs. Going through drying phase alters pulp characteristics in an irreversible manner. Thus dry-broke pulp has different properties than fresh pulp. To ensure even paper quality the fraction of dry-broke pulp in web forming has to be controlled. Broke handling system works as a buffer between dry broke and web forming. (Paulapuro, 2008, pp. 183-189)

During a web break, the broke is pulped, deflaked, cleaned and stored in a broke tower. After that broke is blended with other stock in blend chest. Broke handling can also include various screening, deflaking and additional cleaning stages (Paulapuro, 2008, pp. 13-40). The broke handling system is always designed considering the broke characteristics. For example, wet broke is much easier to disintegrate than dry broke and therefore wet broke pulper and dry broke pulper are completely different by design. In this work a dry broke pulper will be analyzed. (Paulapuro, 2008, pp. 78-84)

Only a few studies have been published regarding pulper development (Demler & Egan 2004; Savolainen et al. 1991). The scarcity of publications is probably due to the sensitive nature of associated product development processes. Savolainen et al. (1991) studied the effect of pulping temperature, consistency and rotor geometry on defibering. They found out that increasing temperature and consistency improved defibering and decreased specific energy consumption. Demler and Egan (2004) simulated vertical pulper using mixing-length model to model turbulence and the properties of water in fluid domain. The simulations were performed to develop new rotor geometry. Simulation predicted rotor power with good accuracy. The rotor that was developed based on simulations was more energy efficient than the original rotor.

4.1 Operating principle

Horizontal pulper consists of vat, chutes, rotor and motor, suction pump, pulp- and water showers and air exhaust. Pulpers usually also have suspension recirculation system. Recirculated suspension is sucked with suction pump through screen plate and directed back to the vat. Suspension recirculation is used when surface level or suspension consistency in pulper has not reached the required level. Recirculation is also used to avoid running suction pump dead-headed. The vat is filled with water to the operation

level before paper web is received. During a web break, paper web is directed to pulper vat with the help of chutes and water showers. Pulp shower is used with heavy paper and board qualities to make sure they sink fast into the pulper. Rotor tears the paper web and agitates the fiber suspension. Fast moving paper web brings even air flow to the pulper during pulping. To avoid pressure rise and excess moisture in pulper air is constantly sucked to the exhaust during pulper operation. Fig. 1 shows a typical structure of a horizontal dry broke pulper.

Paper pulp is sucked through the screen plate during pulping. All pulp is extracted through screen plate during normal operation. Typically, rotor rotation speed, pulp flow rate through screen plate, recirculation and rate of water supply can be controlled during pulper operation. Rotor rotation speed affects pulping and mixing, but also the flow rate of the pulp from pulper. Increasing rotor rotational speed allows for higher flow rate of pulp from vat. Stock level and consistency in pulper should be kept within acceptable level with these control parameters.

4.2 Pulper rotor

Pulper rotor is a critical part of the horizontal pulper since it is responsible for deflaking and mixing of the suspension. The rotor can be seen as a pure shredding device or as a radial pump. Actual rotors have both of these characteristics. Pump specific speed is a useful number in comparing different rotors, especially if the rotor is regarded as a pump type mixer. Pump specific speed is defined as

$$N_q = \frac{\omega\sqrt{Q}}{(gH)^{\frac{3}{4}}}, \tag{4.1}$$

where ω is the rotational speed of the rotor in radians per second, Q is the flow rate in cubic meters per second, H is the total head in meters (Dickenson, 1988, p. 2). Most important rotor design variables are rotor and blade geometry, rotor diameter, number of blades and rotation speed (Savolainen et al., 1991, p. 147; Demler & Egan, 2004, p. 42).

Pulp consistency, retention time, temperature, pH, rotor power per vat volume, used energy, raw material and operation principle are the main parameters in pulping (Valmet Technologies Oy, 2015). All these factors also influence the power consumption of a pulper. The greatest potential for reducing the energy consumption of a pulper is in rotor and screen plate geometry (Demler & Egan, 2004). Rotor uses mechanical power on suspension pumping, paper web shredding and frictional losses. These are factors that can be altered through rotor design. This is why the importance of rotor geometry is pronounced in pulper development. In such project it should be noted that energy saving can’t be the only design criterion when optimizing a pulper rotor.

5. MODELING METHODS

There are no well-established and verified simulation methods for general paper pulp simulations (Cotas, Asendrych, & Rasteiro, 2015; Hämäläinen et al., 2010, pp. 55-58). The modeling methods used in this work are well established in many industrial simulations. The used software and models are used regularly in industrial product development projects. The conflict here is that it is not sure if these methods are capable of accurately simulating processes where paper pulp is the modeled fluid. Different modeling methods are discussed in detail in Section 3.4.

5.1 Geometry and boundary conditions

Geometries of pulper rotors and vat used in this work were provided by Valmet Technologies. Necessary simplification and clean-up procedures were carried out to make the 3D models suitable for meshing. The vat geometry was created with ANSYS DesignModeler. The geometry of the vat is presented in Fig. 6. ANSYS SpaceClaim software was used to clean up the rotor geometries. Moving reference frame domain was created in ANSYS DesignModeler. Moving reference frame made it possible to simulate the flow in a vat as stationary (ANSYS, 2015). The rotor geometries used in this work are presented in Table 1.

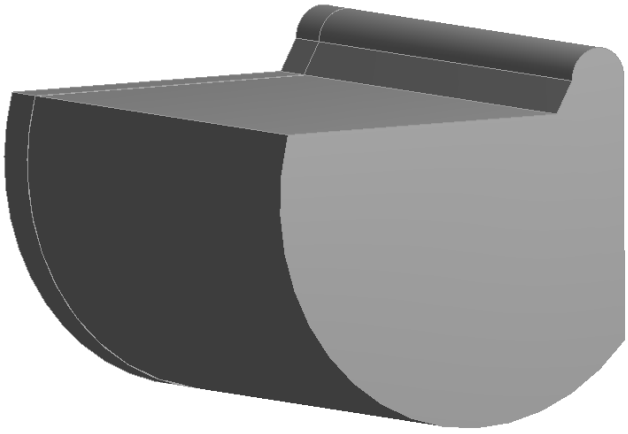

Figure 6. *Three dimensional model of vat geometry.*

Table 1. *Rotor geometries used in simulations.*

Rotor 1	Rotor 2	Rotor 3	Rotor 4	Rotor 5
• 4 pump blades • 8 lower blades	• Geometry of rotor 1 • High pump blades	• Geometry of rotor 1 • Wide pump blades tips	• 5 pump blades • Saw tooth edges on pump blades	• Modified version of rotor 4

Rotor 1 is used in base case simulation. Rotor 2 has higher pump blades compared to rotor 1. Rotor 3 has wider pump blades at the outer peripheral of the rotor than rotor 1. Rotor geometry of rotor 4 is completely different from rotor 1. Rotor 5 is a modified version of rotor 4.

All walls in pulper were specified as no slip walls. In case 7, a symmetry boundary condition was used on one side wall to simulate a case where the pulper is about twice as big and has two identical rotors. The cases are introduced in Section 6, Table 4. A free slip condition was set on surface level of suspension. In reality the surface of suspension in a pulper is a free surface. To simplify simulations, the surface was modeled as uniform surface level. The free slip condition allows the velocity profile to develop in the same direction as it would with an actual free surface boundary condition.

5.2 Solution methods and material model

ANSYS Fluent 17.0 was used as a solver in all simulations. All simulations were performed as three dimensional. Viscous effects were modeled with realizable k-ε turbulence model including enhanced wall treatment. One laminar calculation was also conducted. Laminar case was computationally unstable and convergence was not achieved. Molecular viscosity of suspension near rotor is low due to high shear rate. Turbulence model rises the effective viscosity of fluid near rotor. This stabilizes the calculation. Lack of this stabilizing effect probably led to unstable result in laminar calculation. The results of laminar simulation are not reported in this work. Pressure-Velocity coupling was calculated using coupled solution method. Momentum, turbulent kinetic energy and turbulence dissipation rate were discretized using second order upwind scheme. Gradients were discretized using Green-Gauss node based scheme and pressure using second order scheme. Green-Gauss node based scheme was selected for gradient discretization because it is more accurate than the cell based scheme (ANSYS, 2015). Energy equation was not solved in simulations since heat transfer was not in the scope of this work. Case 4 was simulated as transient. All other cases were simulated as stationary. Transient case could probably be simulated as laminar without big errors since flow values even out in time dependent simulation. LES would likely give even more accurate results than the ones obtained in transient simulation.

Altogether 17 simulations were performed to form a thorough understanding of the flow patterns in the horizontal pulper. Nine surface monitors and three volume monitors were established to monitor the progress of simulations. Rotor moment, average surface velocity, average velocity in the vat and flow rate were found to be the most important monitors. Residuals and monitors were used as convergence criterion during simulations. Simulation was confirmed as converged after sufficiently low residual values and stationary monitor values were reached. In transient simulation the number of iterations per time step was set based on the residual values. Sufficient residual values were achieved on each time step. In steady state cases increasing false time scale factor speeds up the simulation usually with the expense of residual values. During simulations the time scale factor was adjusted to ensure fast convergence and good accuracy.

Herschel-Bulkley material model was used in all simulations. The material parameters published by Mustalahti (2015) were used to determine the parameters in Herschel-Bulkley model. The material model was modified in sensitivity analysis simulations to find out the effect of material model on results. The simulations performed by Mustalahti (2015, pp. 59-63) yielded significant differences compared to measurements. However, there were quite a few uncertainties in measurements and simulation settings; for example, the omission of turbulence model might have a big impact on the results. It should also be noted that Ansys CFX 14.5 has a simplistic version of Herschel-Bulkley model compared to Fluent 17.0 (ANSYS, 2015).

5.3 Mesh

All meshes used in simulations were created with ANSYS Mesh software. The mesh was refined in the moving reference frame domain and inflation layers were created on all surfaces. At first case the mesh consisted of around 5 million elements. The maximum skewness of the elements was well below 0.9 and other element quality criterions were also on good level. Named selections were also created to simplify solver setup procedures. The mesh was converted to polyhedral mesh in Fluent. Polyhedral mesh gives more accurate gradient approximations. Due to this the amount of elements can be reduced significantly without reducing the quality of the mesh. After conversion to polyhedral the amount of elements was reduced to around 1.4 million. For each rotor type an equivalent mesh was created. The meshing parameters were the same as in case 1, but different rotor geometries resulted in slightly different mesh sizes.

To study mesh independence a coarser version of the case 1 mesh was created. The coarse mesh had around 4.4 million elements. The principle of creating the mesh remained the same. Only element size was changed. The coarse mesh was also converted to a polyhedral mesh. After conversion the mesh composed of around 1.2 million elements. Results of simulation with coarse mesh are presented in Table 2. The results are presented in relation to case 1.

Table 2. *Results of mesh independency study.*

	Rotor power	Average surface velocity	Average velocity in vat	Flowrate	Rotor efficiency
Coarse mesh	1.000	0.994	0.997	1.000	1.001
Difference	0.04 %	0.62 %	0.33 %	0.01 %	0.09 %

The results of mesh independence study clearly prove that the simulation is mesh independent. However, the original finer mesh was used in all following simulations to make sure that the changes in material model do not provoke mesh related computational problems.

5.4 Quantities describing pulper performance

In a broke pulper three main features determine the performance of a pulper. These are pulper's ability to introduce paper web to the suspension, ability to mix the suspension effectively and ability to slush paper web. If these three preconditions are fulfilled the pulper works as desired. In a sense energy efficiency can also be seen as a performance criterion in pulper evaluation. Energy efficiency does not necessarily affect the pulping performance, but it is essential when the whole pulping process is examined. Savolainen et al. (1991) used Somerville shieves and Specific Energy Consumption (SEC) to analyze pulping performance. Somerville shieves cannot be predicted based on CFD simulation. The SEC value can be calculated based on CFD simulation only for batch type pulping process if the pulping time is known. To measure and compare the performance of different pulper setups six quantities were established. Four of these are volumetric quantities. First volumetric quantity is the volume in pulper where the velocity of pulp is over 0.1 m/s. Second quantity is the volumetric flow rate leaving the rotor. Rest volumetric quantities are volumes in pulper where turbulence dissipation rate, shear rate or shear stress exceed certain threshold. Last quantity is the hydrodynamic rotor efficiency. Also average velocities in vat and on vat surface were used to evaluate pulper performance. Pulper features and the performance evaluation criteria that describe them are presented in Table 3. The motivation for the partition shown in Table 3 is presented in Section 6.

Table 3. *Pulper features and the associated performance indicators.*

Ability to introduce paper web to suspension	Mixing	Deflaking	Efficiency
• Average surface velocity • Suction depth, not simulated	• Average velocity in vat • Flow rate from rotor • Volume of velocity over 0.1 m/s	• Shear rate • Shear stress • Turbulence dissipation rate	• Hydrodynamic rotor efficiency

Volumetric flow rate, hydrodynamic rotor efficiency and volumetric threshold integrals are calculated as described in equations 5.1, 5.4 and 5.5, respectively. Also volumes in pulper where turbulence kinetic energy exceeds certain threshold were calculated. The flow rate from rotor is calculated as follows:

$$Q = \int_{MRF} \underline{u}_{rad,pos} \cdot \underline{dA} \ , \tag{5.1}$$

where $\underline{u}_{rad,pos}$ is positive radial velocity. Shaft power and the power extracted from rotor to flow were calculated to determine rotor efficiency. Shaft power was calculated as

$$P_{shaft} = \int_{Rotor} \underline{\omega} \cdot (\underline{r} \times \underline{f}) \, dA \, , \tag{5.2}$$

where $\underline{\omega}$ is angular velocity vector, $\underline{r}$ is radius vector and $\underline{f}$ is the force vector. Force vector consists of pressure force vector and viscous force vector (ANSYS, 2015). The power going from rotor to flow is defined as:

$$P_{flow} = \int_{MRF} \left(p_s + \frac{1}{2} \rho |\underline{u}|^2 \right) \underline{u} \cdot d\underline{A} \, , \tag{5.3}$$

where p_s is static pressure. Now we can define the rotor efficiency as follows:

$$\eta_{rotor} = \frac{P_{shaft}}{P_{flow}} \tag{5.4}$$

Threshold integrals are calculated as follows:

$$V_{\Phi,over\ \Phi_{thr}} = \int_{Vat} \frac{\Phi - \Phi_{thr} + |\Phi - \Phi_{thr}|}{2(\Phi - \Phi_{thr})} dV \ , \tag{5.5}$$

where Φ is the value of quantity and Φ_{thr} is the threshold value. For pulper performance comparison the shear stress is defined as

$$\tau = \mu_{\text{eff}} \dot{\gamma} \ . \tag{5.6}$$

Turbulence dissipation is calculated from Eq. 3.12 and turbulence kinetic energy is calculated from Eq. 3.13. Shear rate is calculated as defined in Eq. 2.5. Shear rate, turbulence dissipation rate and turbulence kinetic energy are predefined quantities in ANSYS Fluent 17.0. These quantities can be read straight from the simulation software.

5.5 Suspension treatment regimes

Suspension treatment can be divided to four categories based on the mechanical energy introduced to the suspension. These categories are mixing, deflaking, deflocculation and defibering. In low intensity mixing the fiber flocs in suspension do not disperse, but the flocs move in relation to each other. Power dissipation level in mixing is below the onset of fluidization of suspension. This threshold value depends on the consistency of suspension, but for a 4 % suspension the threshold value is around 53 kW/m^3 (Bennington & Kerekes, 1996). Length scale of mixing is the size of vat, which is in the scale of 1-10 m.

Deflocculation length scale is the size of a typical flock. Flock diameter is usually around 1 cm. Power dissipation in deflocculation is the same as needed for suspension fluidization. Deflaking length scale is the size of paper flakes in suspension. This length scale is around 2-15 cm. Power dissipation in a typical deflaker is around 6000 kW/m^3 (Voith Paper, 2016). Defibering length scale is the length of typical wood fiber, which is 1-3 mm (Derakhshandeh et al., 2011, p. 3461). Defibering happens mainly in refiners, where power dissipation is significantly greater than in pulpers and deflakers. Different suspension trestment regimes are presented in Fig. 7. Power dissipation as a quantity is more suitable for describing small-scale mixing than large scales (Bennington, 1988, s. 32).

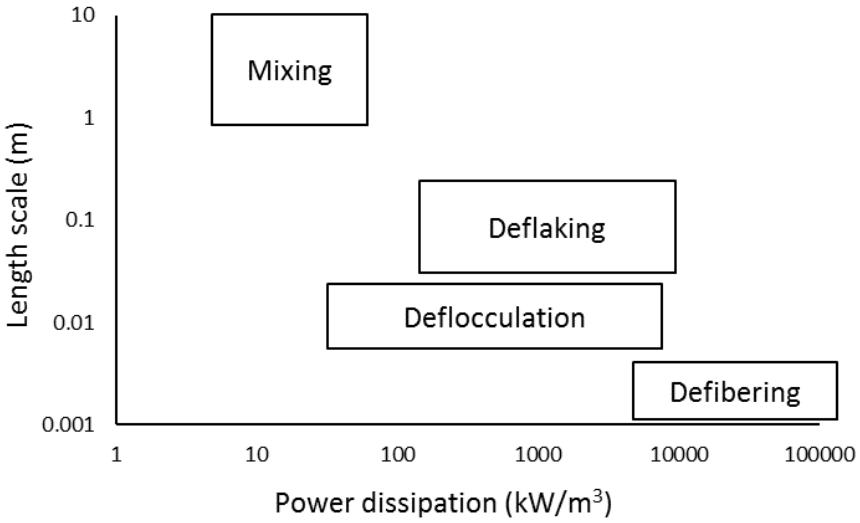

Figure 7. *Suspension treatment regimes.*

6. RESULTS

Results of the simulated cases were collected in consistent manner to make the comparison of results easy. The post-processing of results was also done with same template in all cases. In this chapter the results of the CFD simulations are presented. The results of mesh independency study are presented in Section 5.3. The simulated cases are listed in Table 4.

Table 4. *List of simulated cases.*

Case number	Rotor	Material model	Other design parameters
1	Rotor 1	Mustalahti	
2	Rotor 1	Mustalahti	45 degrees rotated
3	Rotor 1	Water	
4	Rotor 1	Mustalahti	Transient simulation
5	Rotor 1	Mustalahti	Consistency 5 %
6	Rotor 1	Mustalahti	Consistency 6 %
7	Rotor 1	Mustalahti	Symmetry boundary
8	Rotor 1	Mustalahti	370 rpm
9	Rotor 2	Mustalahti	
10	Rotor 3	Mustalahti	
11	Rotor 4	Mustalahti	
12	Rotor 4	Mustalahti	299 rpm
13	Rotor 5	Mustalahti	
14	Rotor 1	Mustalahti, 1.05× n	
15	Rotor 1	Mustalahti, 1.05× k	
16	Rotor 1	Mustalahti, 1.05× τ_y	
17	Rotor 1	Mustalahti, 1.05× $\dot{\gamma}_c$	

In Table 4 the 45 degrees rotation refers to the rotational position of the rotor in a stationary calculation. Velocity distribution in the vat in the base case was closer to transient results than in the 45 degrees rotated case. Thereby, the original rotor position was used in all following stationary simulations. Symmetry boundary refers to the boundary condition on the left side of the vat. Symmetry boundary condition simulates the case with 2 rotors in a vat roughly twice the size of the original vat. All cases, except for cases 8 and 12, were simulated with 318 rpm rotational speed.

6.1 Flow rate, mixing and efficiency

Flow rate and rotor efficiency can be calculated directly from the simulation results. However, additional quantities need to be defined to evaluate mixing. In this work average surface velocities, average velocities in vat, velocity contours and volumes of suspension moving over 0.1 m/s were used to describe mixing.

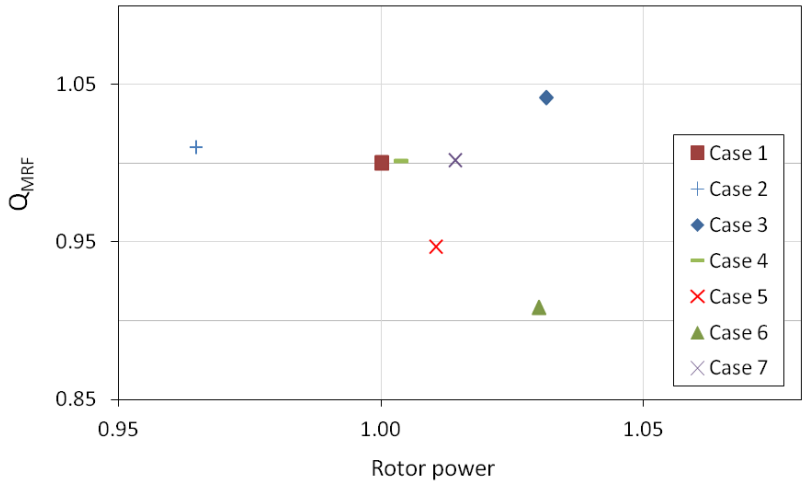

Figure 8. *Flow rate versus rotor power in cases 1-7.*

If flow pattern on the vat surface is approximately constant, then average surface velocity can be used to describe pulper's ability to introduce paper web to the suspension. Average velocity in the vat can be seen as a similar indicator. However, average velocity in vat describes more mixing in vat than the ability to introduce paper web to the suspension. Flow rates, rotor powers and efficiencies were calculated as described in Section 5.5. All results in this chapter are reported in relation to the case 1 results. Thus the values from case 1 are always 1. This makes comparing different cases easier.

Flow rates versus rotor power relative to case 1 in cases 1-7 and 8-13 are presented in Figs. 8 and 9, respectively. Note the different scales in figures. Rotor power in case 2 is slightly lower and flow rate slightly larger than in case 1. This might be caused by the different rotational position of rotor in these cases. The flow resistance seems to be greater in the position used in case 1. It is clear that the rotor power increases and flow rate decreases when suspension consistency is raised. This can be seen in cases 5 and 6. The result of transient simulation in case 4 is virtually the same as in case 1, which proves that the stationary simulations are accurate when it comes to flow rate and rotor power. Simulation with water in case 3 yielded surprisingly similar results with case 1.

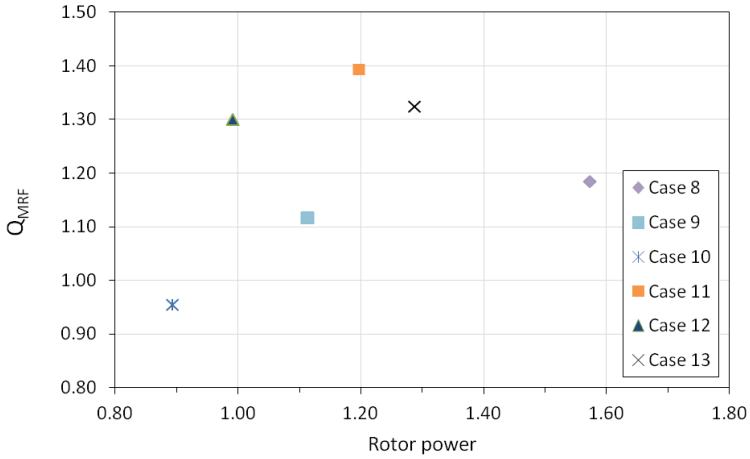

Figure 9. *Flow rate versus rotor power in cases 9-13.*

High pump vanes in case 9 resulted in about 10 % higher rotor power and flow rate than in case 1. Rising rotational velocity to 370 rpm increases rotor power significantly even tough flow rate increases under 20 %. Wider pump blade tips decrease both flow rate and rotor power. All other rotor designs improve relative flow rate more than they increase rotor power.

Average surface velocities and flow rates seem to have a connection. Increasing flow rate increases also average surface velocity. The relation of surface velocity and flow rate is not straightforward. Case 11 has the highest flow rate in this study, but the average surface velocity is only third largest. In case 13 flow rate is lower than in case 11, but the average surface velocity is higher than in any other case. High average surface velocity in case 13 is probably due to greater rotational component in flow in case 13 than in case 11. Thus pulper's ability to introduce paper web to the suspension might not always increase as the average surface velocity increases. High flow rate and high average surface velocity are together a strong indication of good ability to introduce paper web to the suspension. Average surface velocity versus rotor power in cases 1-7 and 8-13 are presented in Figs. 10 and 11, respectively.

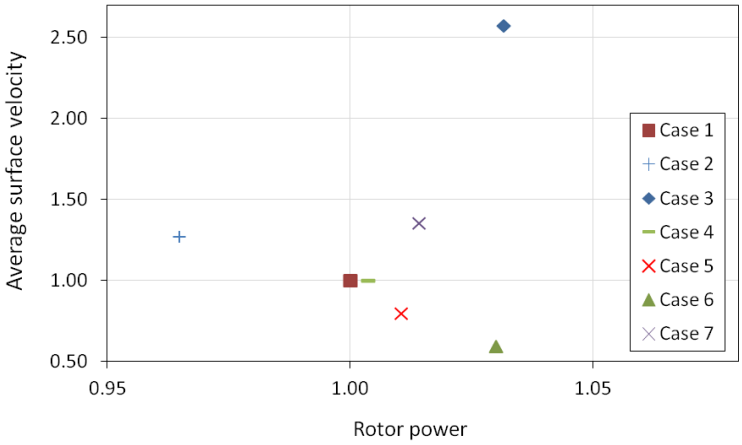

Figure 10. *Average surface velocity versus rotor power relative to case 1 in cases 1-7.*

The difference in flow rate and surface velocity is pronounced in case 3, because the viscosity of water is mostly lower than viscosity of paper pulp. Cases 5 and 6 clearly demonstrate that increasing consistency decreases surface velocities in the vat. This means that rising consistency in pulper probably weakens the pulper's ability to introduce paper web to the suspension. It seems that both rotor 2 in case 9 and rotor 4 in case 12 would introduce paper web to the suspension better than rotor 1 in case 1. Rotor efficiency was calculated in all cases as described in Section 5.4. In cases 1-7 the rotor efficiencies land in a margin of 3 %. This indicates that the way of calculating rotor efficiency is valid, since theoretically there should not be differences in rotor efficiencies in cases 1-7. Rotor efficiency versus rotor power in cases 1-7 and 8-13 are presented in Figs. 12 and 13, respectively.

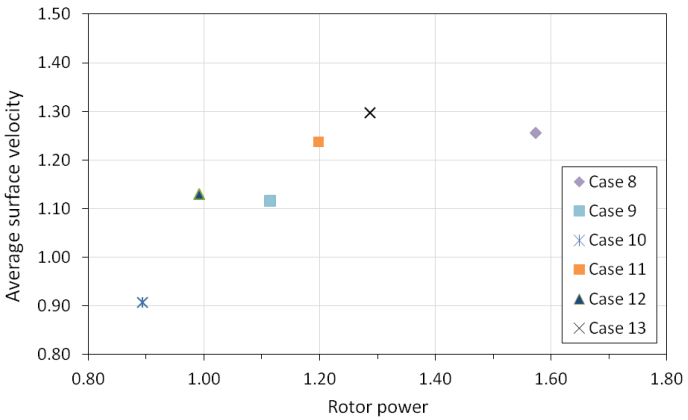

Figure 11. *Average surface velocity versus rotor power relative to case 1 in cases 8-13.*

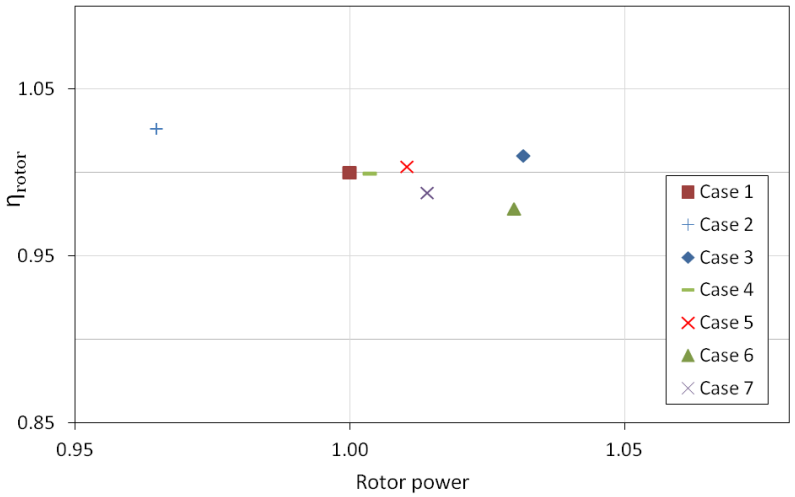

Figure 12. *Rotor efficiencies versus rotor power relative to case 1 in cases 1-7.*

Increased rotor rpm does not affect rotor efficiency in case 8. The same trend can also be seen when comparing cases 11 and 12. High pump vanes increase efficiency about 3 %. Wide pump vane tips worsen rotor efficiency a little. Rotors 4 and 5 have clearly better efficiency than rotor 1. Rotor 4 has over 14 % better efficiency than rotor 1 in case 1. Average velocity in the vat seems to be linked to flow rate in the same way as average surface velocity. Cases with high flow rate tend to have high average velocity in vat. Cases 11 and 13 have same average velocity in vat, but rotor power is higher in case 13 than in case 11. This indicates that rotor 5 is less efficient in mixing than rotor 4. High velocity in vat with high flowrate and average surface velocity in case 12 indicates that rotor 4 also has good ability to introduce paper web to the suspension. Average velocity in vat versus rotor power in cases 1-13 is presented in Fig. 14.

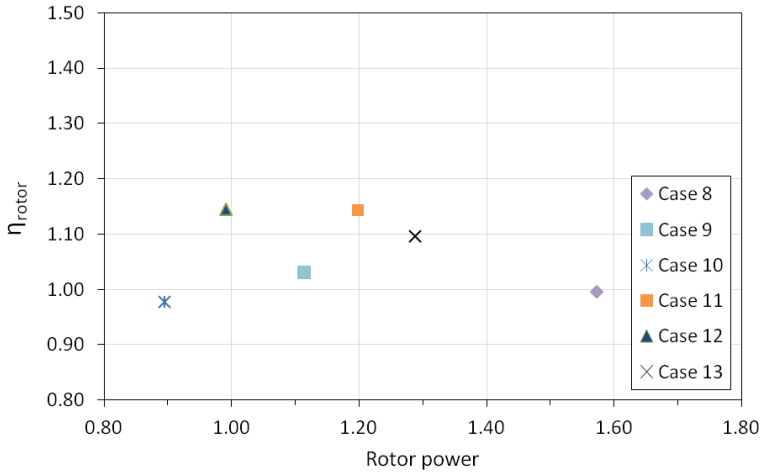

Figure 13. *Rotor efficiencies versus rotor power relative to case 1 in cases 8-13.*

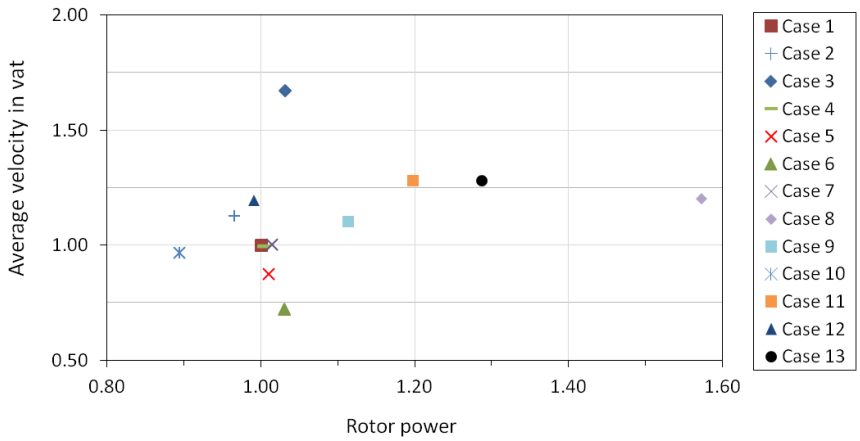

Figure 14. *Average velocity in vat versus rotor power relative to case 1 in cases 1-13.*

Volume integral of areas where velocity is over 0.1 m/s is somewhat complex quantity. This variable is not necessarily a really good indicator for pulp mixing, since the areas where velocity falls below 0.1 m/s are typically located near walls. Thus the value of the integral might rise only slightly even if mixing is dramatically improved. However, the rise in this volumetric quantity always predicts better mixing. Hence it can be useful when comparing different pulper setups. Volume of areas where velocity is over 0.1 m/s in vat versus rotor power in cases 1-13 are presented in Fig.15. It should be noted that in case 1 the velocity is under 0.1 m/s only in a small fraction of the vat volume. The differences in volumes of over 0.1 m/s velocity are really small. Only cases 3, 5, 6 and 7 stand out in the graph. It is not surprising that the share of low velocity in vat is smaller when water is used as a fluid instead of the paper pulp. On the contrary it is surprising that the volume of suspension moving over 0.1 m/s is lowest in case 7.

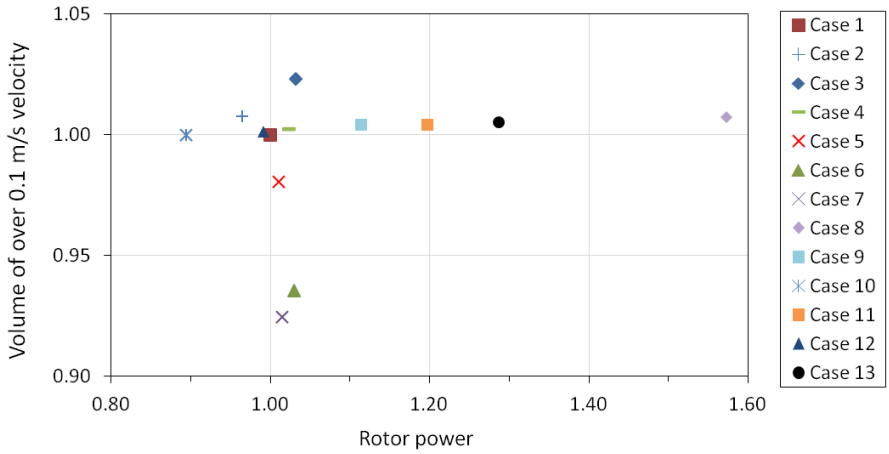

Figure 15. *Volume of areas where velocity is over 0.1 m/s versus rotor power relative to case 1.*

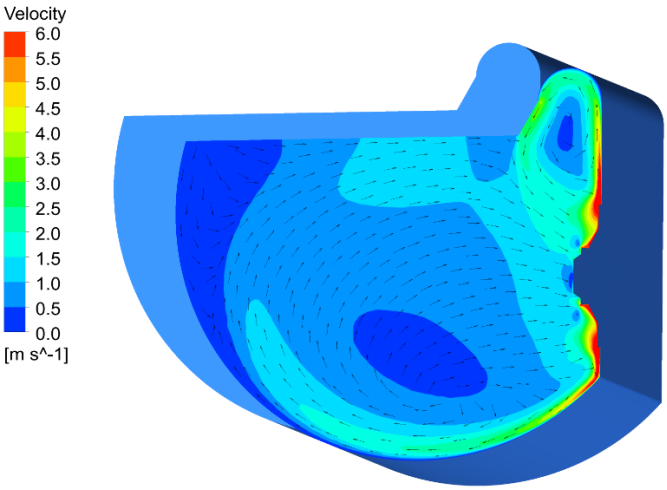

Figure 16. *Velocity contour in vat cross-section in case 1.*

This might be due to low rotor power and uneven flow distribution in the vat. Cases 5 and 6 show that increasing consistency increases also the volume of stagnant suspension in the pulper.

Mixing in vat was estimated also based on velocity contours in vat cross-sections. From Fig. 16 can be seen that the whole vat is mixed in case 1. The areas where velocity is between 0.5 m/s and 0 m/s are quite small and even there the suspension is probably not completely stagnant. Rising pulp consistency slows down the suspension movement in whole pulper when compared to case 1. This can be seen when comparing Figs. 16 and 17. The area of slowly moving suspension is significantly larger in case 6 than in case 1.

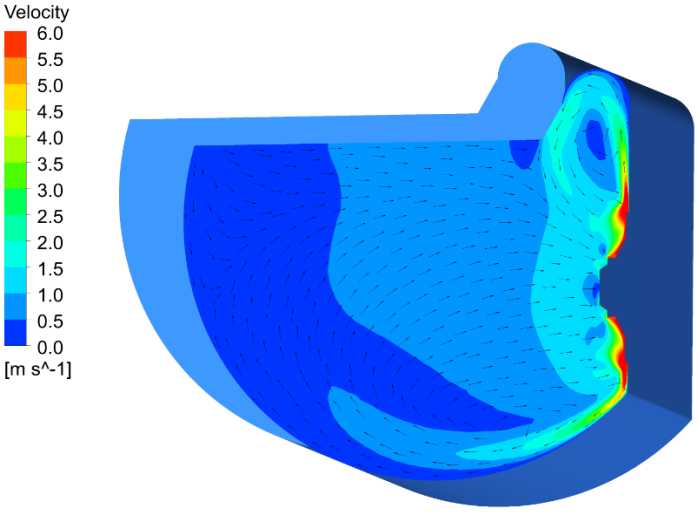

Figure 17. *Velocity contour in vat cross-section in case 6.*

In case 12 the velocities in cross-section are higher than in case 1. Velocity contour in vat cross-section in case 12 is presented in Appendix A, Fig. A1. The areas where suspension moves slowly are smaller in case 12 than in case 1. This supports the theory that rotor 4 generates better mixing in the vat than in rotor 1 with same power input.

The rotational position of rotor affects velocity distribution of a stationary simulation. Figs. 18 and 19 show that 45 degrees change in rotor rotational position changes the flow field significantly. In case 1 a small vortex seems to develop in the upper left corner of vat. The vortex might actually be there, but its size and strength are probably overpredicted. The vortex is not present in transient simulation, but flow conditions in the area would favour vortex formation. In case 2 (Fig. 19) there is no vortex in upper left corner, but a small vortex develops in lower left corner. Transient simulation shows no vortex in lower left corner. Transient simulation gives the most reliable velocity distribution results. The velocity distribution in case 4 (Fig. 20) is more even than in cases 1 and 2. From this we can conclude that stationary simulations do not predict the exact flow field correctly.

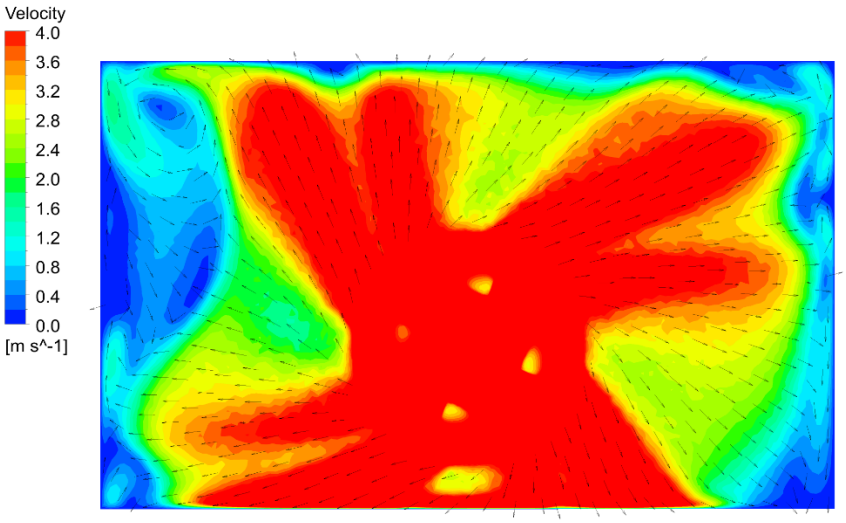

Figure 18. *Velocity contour 5 cm from back wall in case 1.*

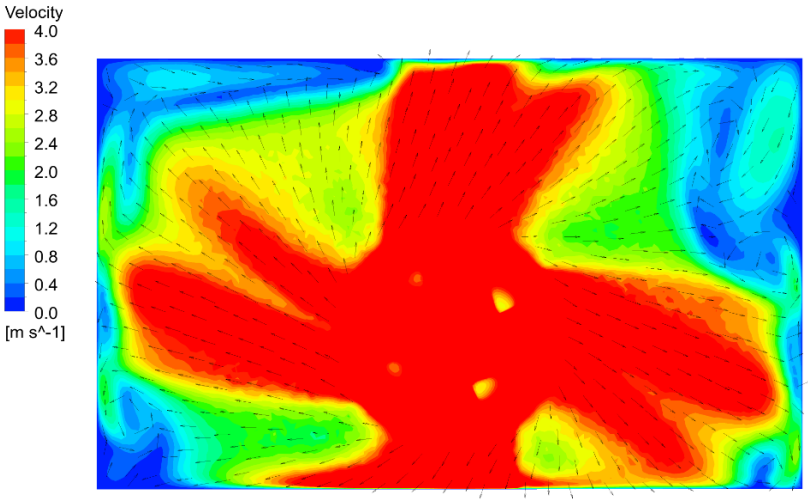

Figure 19. *Velocity contour 5 cm from back wall in case 2.*

Velocity distribution is quite even in case 12, since there is one pump blade more than in rotor 1. Also the rotor geometry supports more even velocity distribution. Transient simulation might not yield much different velocity distribution with rotor 4. Based on velocity contours the mixing is better with rotor 4 in case 12 than with rotor 1 in transient simulation. Velocity contour 5 cm from back wall in case 12 is presented in Appendix A, Fig A2. Rotor 4 seems to perform better than rotor 1 in all areas reviewed in this section.

In some simulations fluid surface level can be predicted from pressure distribution on simulated surface level. This could help in simulating the paper web sinking in a horizontal pulper. However, in pulper simulations pressure distribution on the free surface of vat was highly affected by the free surface geometry. Thus no reliable prediction of surface level could be done based on surface pressures. Pressure contour on free surface of vat in case 1 is presented in Fig. 21.

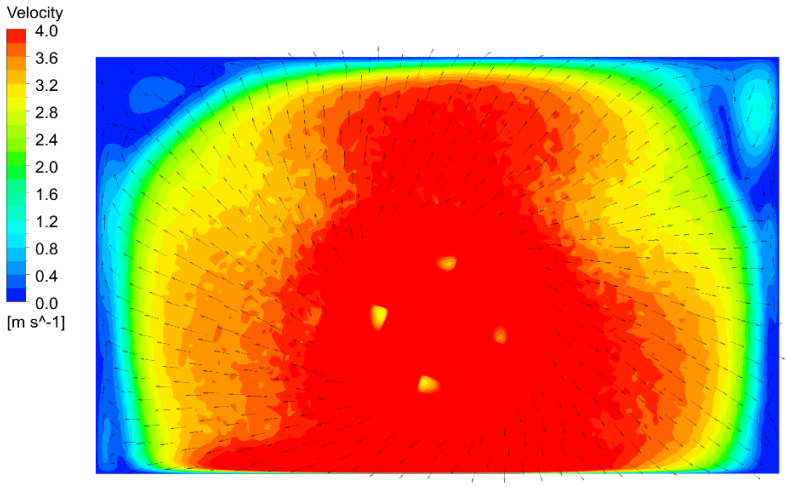

Figure 20. *Velocity contour 5 cm from back wall in transient simulation.*

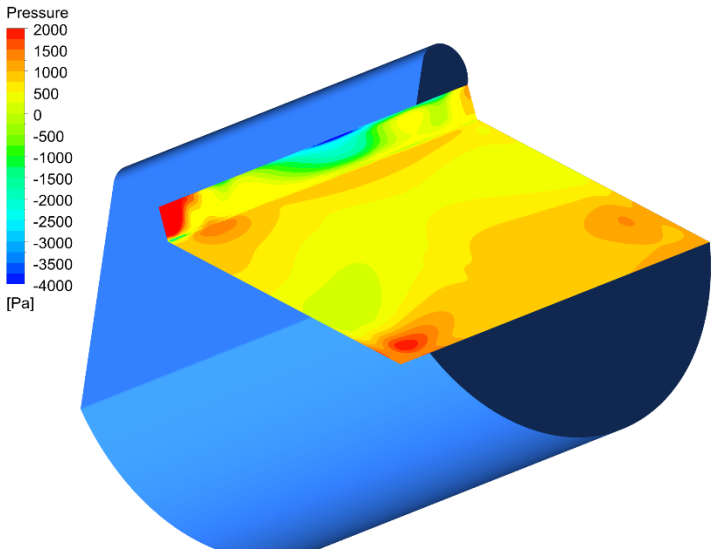

Figure 21. *Pressure contour on free surface of vat in case 1.*

6.2 Quantities describing pulping performance

Pulping performance can be determined as pulper's ability to slush paper web once it is introduced to the suspension. Three of the six quantities introduced in Section 5.4 describe pulping performance; these are volumes in pulper where turbulence dissipation rate, shear rate or shear stress exceed certain threshold. Also, volume where turbulence kinetic energy exceeds certain threshold value was used to evaluate pulping performance.

6.2.1 Turbulence dissipation rate

Power dissipation rate has been identified as a good measure to quantify fiber suspension fluidization and flock dispersion (Olson, 2005, p. 9; Bennington & Kerekes, 1996). Power dissipation itself is not the cause of fluidization, but the turbulent shear caused by it. Turbulence dissipation is part of the total power dissipation in flow. However, in pulpers the flow near rotor area is highly turbulent. Also one definition of fluidization is that the suspension flow is fully turbulent (Bennington & Kerekes, Power requirements for pulp suspension fluidization, 1996, p. 254). Due to this it is justified to use turbulence dissipation rate to asses pulping performance of a pulper.

Many threshold values and correlations have been determined for paper pulp fluidization (Bennington & Kerekes, Power requirements for pulp suspension fluidization, 1996). Reported threshold values for fluidization vary significantly. For example, power dissipation values for fluidization of 4 % pulp suspension, that has density of 1000 kg/m^3, are 38 W/kg, 53 W/kg, 163 W/kg and 1440 W/kg (Bennington & Kerekes, 1996; Olson, 2005, p. 10). The large scale of threshold values results from different definition of fluidization.

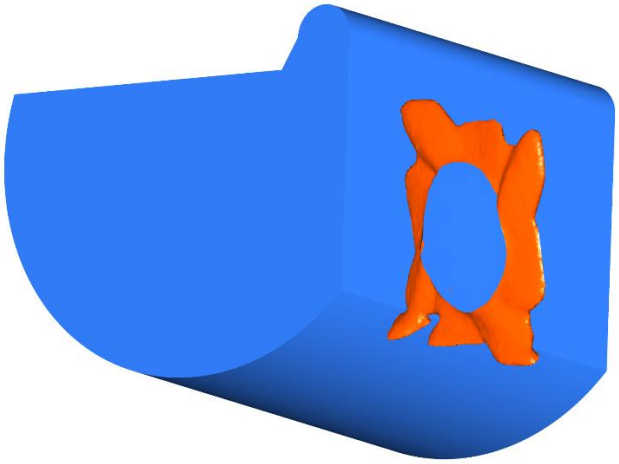

Figure 22. *Isosurface of turbulence dissipation rate 53 W/kg in case 1.*

In this work turbulence dissipation rates from 50 W/kg to 300 W/kg are used to describe pulping. It should be noted that total power dissipation in a pulper is greater than turbulence dissipation. This is why the range of turbulence dissipation values used in this work does not reach the highest threshold values reported in the literature.

The isosurfaces of turbulence dissipation rate 53 W/kg in cases 1 and 12 are presented in Figs. 22 and 23, respectively. In the case 1 large portion of the volume of power dissipation exceeding 53 W/kg is in Moving Reference Frame (MRF) domain. In case 12 the corresponding area is mainly outside MRF. Turbulence dissipation isosurface in MRF domain is not shown in Figs. 22 and 23. The volume of power dissipation exceeding 53 W/kg is about 26 % larger in case 12 than in case 1.

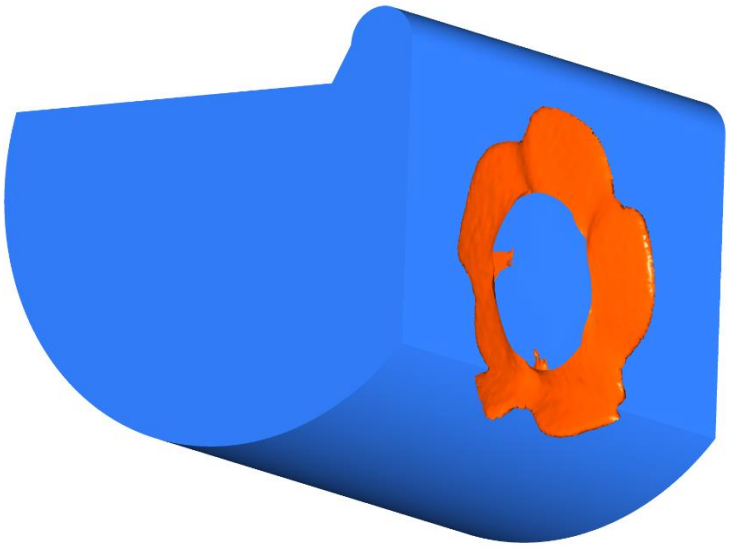

Figure 23. *Isosurface of turbulence dissipation rate 53 W/kg in case 12.*

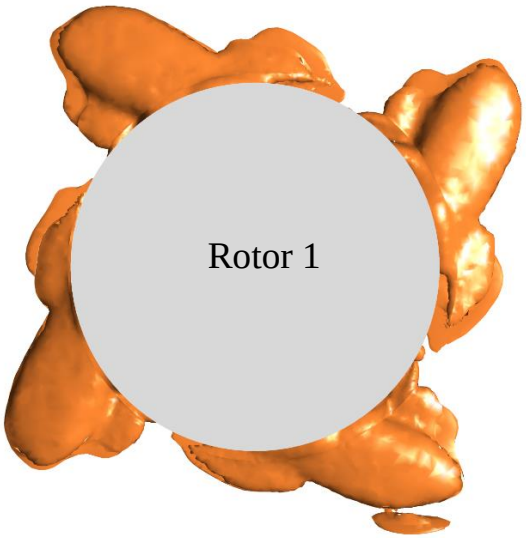

Figure 24. *Isosurface of turbulence dissipation rate 200 W/kg in case 1.*

The isosurface of turbulence dissipation rate 200 W/kg in cases 1 and 12 is presented in Figs. 24 and 25, respectively. Surprisingly rotor 4 in case 12 has 52 % smaller volume of power dissipation exceeding 200 W/kg than rotor 1 in case 1. Low volume of high intensity turbulence dissipation rate in case 12 might be due to the high rotor efficiency of rotor 4. Efficient rotor is likely to produces less turbulence in flow than a rotor with low efficiency. This means that also turbulence dissipation rate is low. Based on turbulence kinetic energy results in Section 6.2.4 rotor 4 seems to produce less high intensity turbulent energy than rotor 1. Studying total power dissipation could provide more comprehensive understanding of the case.

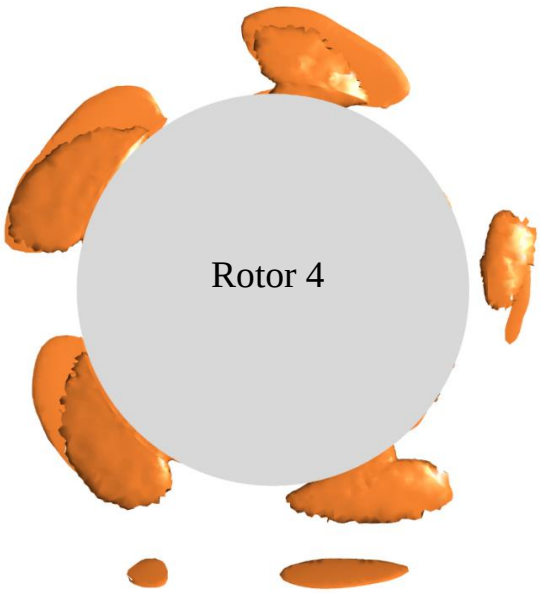

Figure 25. *Isosurface of turbulence dissipation rate 200 W/kg in case 12.*

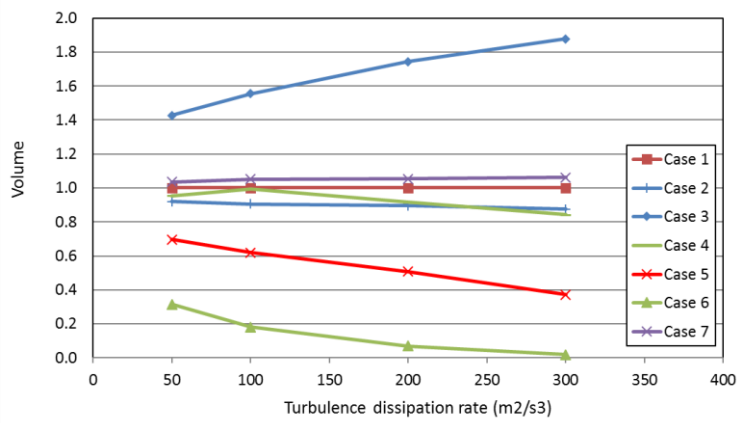

Figure 26. *Turbulence dissipation rate isovolumes relative to case 1 in cases 1-7.*

Turbulence dissipation rate isovolumes in cases 1-7 and 8-13 are presented in Figs. 26 and 27, respectively. Turbulence dissipation isovolumes are higher in case 3 than case 1 and the difference increases with higher threshold values. This results from the low viscosity in case 3. High consistency in cases 5 and 6 leads to low volumes of turbulence dissipation isovolumes. Isovolumes in all remaining cases do not differ much from case 1. This is not surprising, since the differences between cases 1, 3, 4 and 7 are small. Rotors 4 and 5 in cases 11, 12 and 13 create relatively small turbulence dissipation isovolumes in high threshold values. Rotor 2 seems to perform better than rotor 1 on whole turbulence dissipation rate range. It is not surprising that high rpm in case 8 results in high turbulence dissipation rate. High rotational speed creates typically more high intensity turbulence. Thus it is logical that isovolumes in case 8 grow relative to case 1 as dissipation rate threshold rises.

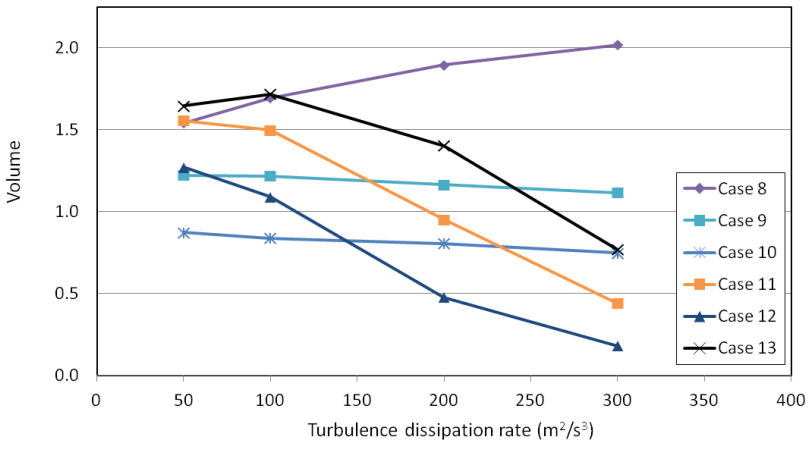

Figure 27. *Turbulence dissipation rate isovolumes relative to case 1 in cases 8-13.*

6.2.2 Shear rate

In experimental studies flock dispersion has been found to happen in extension flow and when shear was applied to flocs by a physical contact (Derakhshandeh et al., 2011, p. 3466). The velocity derivatives that describe extension flow are taken into account in the definition of shear rate, as described in Section 2.1. This is why shear rate could be a good quantity to describe pulping. Shear rate can be calculated directly in Fluent 17.0. Shear rate values and shear rate isovolumes are however highly affected by walls and wall geometry. Areas of high shear rate are typically located near walls. This can distort a shear rate based pulping performance comparison. If the geometry is not altered, then shear rate can be a good performance indicator. In pulper simulations only rotor geometry was changed, so shear rate comparison should give a reasonable understanding of pulping performance. Isosurface of shear rate over 100 1/s in case 1 is presented in Fig. 28. Shear rate levels in pulper simulations were analyzed with threshold integrals. Shear rate isovolumes in cases 1-7 and 8-13 are presented in Figs. 29 and 30, respectively. Shear rate isovolumes in cases 2 and 4-7 resemble turbulence dissipation rate isovolumes when comparing different cases. Simulation with water in case 3 yielded much lower shear rate values than case 1. This is due to the low viscosity of water. Shear rate isovolumes indicate same kind of pulping performance as turbulence dissipation in cases 8-10.

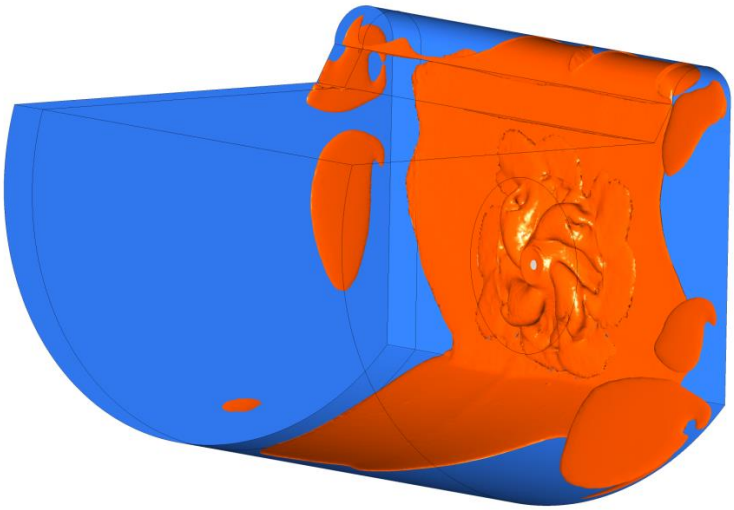

Figure 28. *Isosurface of shear rate over 100 1/s in case 1.*

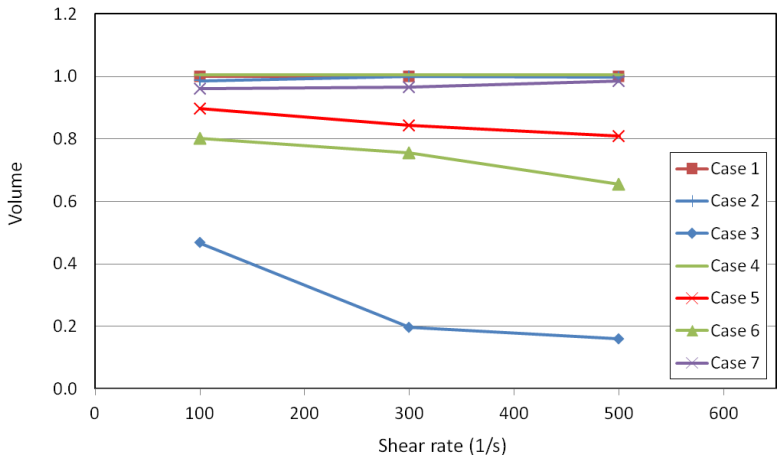

Figure 29. *Shear rate isovolumes relative to case 1 in cases 1-7.*

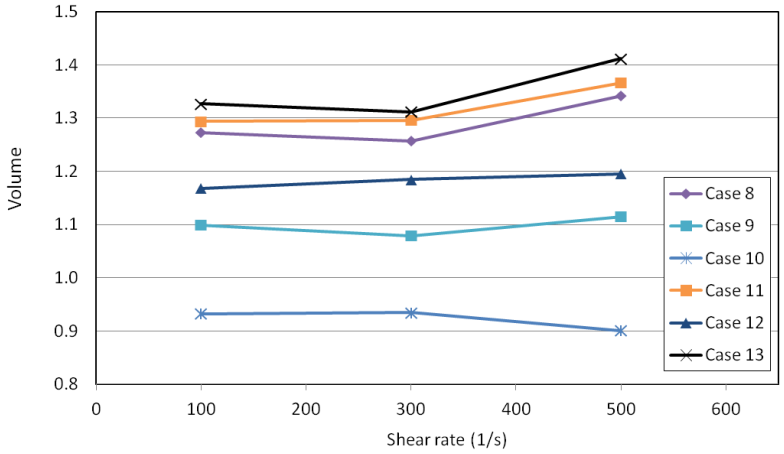

Figure 30. *Shear rate isovolumes relative to case 1 in cases 8-13.*

6.2.3 Shear stress

Extension flow and turbulent shear promote defibering (Derakhshandeh, et al., 2011, p. 3466; Olson, 2005). In one dimensional shear flow shear stress is defined as a product of shear rate and effective viscosity. In real three dimensional flow shear rate includes the effect of extension flow and effective viscosity includes turbulent viscosity. This is why shear stress is potentially a good measure of pulping performance. Areas of high shear rate develop on rotor edges, in high speed flow from rotor, on the suction side of pump blades and near the vat walls where flow speed is high. Shear stress was calculated as described in Eq. 5.6. This is not a physical quantity, but it represents the magnitude of shear stress. Shear stress isovolumes in cases 1-7 and 8-13 are presented in Figs. 0 and 32, respectively. It is a bit surprising that shear stress isovolumes in case 2 are notably smaller than in case 1. This might be due to the different velocity distribution in vat.

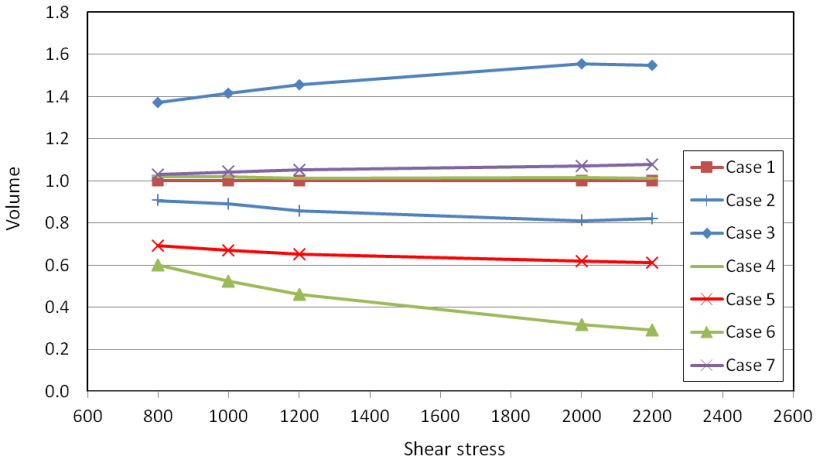

Figure 31. *Shear stress isovolumes relative to case 1 in cases 1-7.*

In case 3 the isovolumes seem to be much higher than in case 1. This is probably caused by a computational error. Shear rate levels are much lower in case 3 than in case 1 and the effective viscosity is also lower in case 3 than in case 1. Thus it is not logical that the isovolumes of shear stress would be larger in case 3 than in case 1.

Rotor 1 at 370 rpm (case 8) and rotors 4 (case 11) and 5 (case 13) at 318 rpm are in the same performance range in terms of shear stress isovolumes. Rotor 4 at 299 rpm (case 12) and rotor 2 at 318 rpm (case 9) are also really close in this comparison. This means that high pump vanes and design of rotor 4 seem to be good in terms of pulping performance. However, turbulence dissipation indicated that rotor 4 at 299 rpm was not as effective in pulping as rotor 2 at 318 rpm. As mentioned in Section 6.3.1, the high efficiency of rotor 4 might cause low turbulence level in pulper.

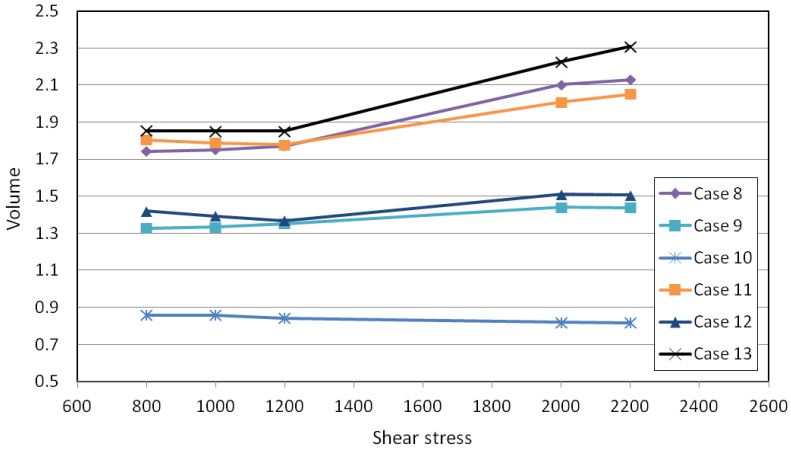

Figure 32. *Shear stress isovolumes relative to case 1 in cases 8-13.*

6.2.4 Other quantities

Turbulence kinetic energy is a useful quantity in pulper simulations, since it depicts the level of turbulence the rotor creates. Turbulence kinetic energy can also be helpful when evaluating turbulence dissipation rate results. Isosurface of turbulence kinetic energy 5 m^2/s^2 in case 1 is presented in Fig. 33. It seems that the flow in vat is turbulent only near the rotor. This is in line with the simulations concluded by Huhtanen (2004, p. 90) for a mixer. Turbulence kinetic energy isovolumes in cases 1-7 and 8-13 are presented in Figs. 34 and 35, respectively. Turbulence kinetic energy values are slightly larger in the simulation with water (case 3) than in case 1. This is logical, since pulp tends to dampen turbulence. It is a bit surprising that transient simulation (case 4) yields about 20 % smaller turbulence kinetic energy isovolumes than stationary simulation. This might be linked to the more even velocity distribution of transient simulation. It can be seen from Fig. 35 that the turbulence kinetic energy isovolumes of rotors 4 and 5 fall quite sharply as the kinetic energy threshold exceeds 7 m^2/s^2. The trend would probably continue if the turbulence kinetic energy threshold was further increased. This strengthens the conclusion that rotors 4 and 5 do not produce as much high intensity turbulence as rotor 1 on same power input.

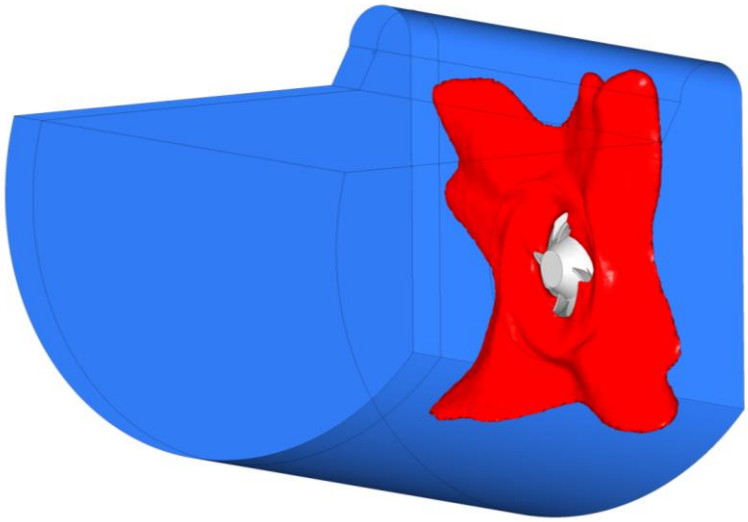

Figure 33. *Isosurface of turbulence kinetic energy 5 m^2/s^2 in case 1.*

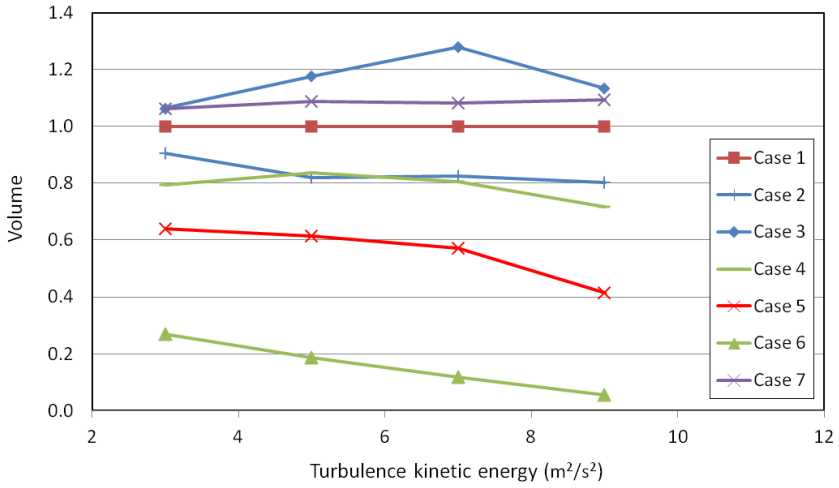

Figure 34. *Turbulence kinetic energy isovolumes relative to case 1 in cases 1-7.*

Velocity streamlines in MRF were used to visualize flow patterns near rotor. Flow pattern near rotor can reveal unwanted flow behaviour like flow separation. In case 1 a vortex-like curl develops behind pump blade. The flow is clearly directed towards the lower blade. The vortex-type curved flow and flow direction to low blade could be the reasons of high intensity turbulence generation. In case 12 the velocity streamlines over pump blade distributes smoothly to the space between blades. The flow behaves as if there was a diverging channel. The vortex-like curved streamlines are not as pronounced as in case 1. Velocity is high near blade tip, where flow leaves the rotor. The smooth behaviour of flow on rotor 4 could explain the small share of high intensity turbulence.

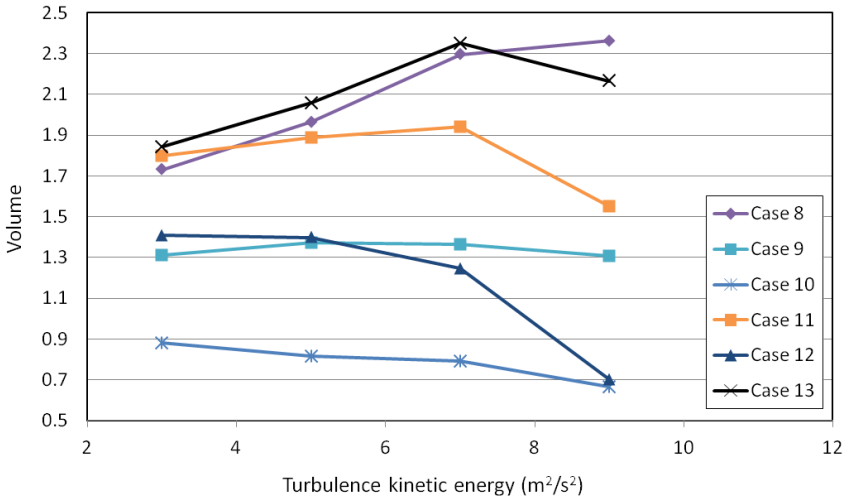

Figure 35. *Turbulence kinetic energy isovolumes relative to case 1 in cases 8-13.*

6.3 Sensitivity analysis of material model

The sensitivity of results in terms of material model parameters was determined analytically and using CFD. In both cases, the parameters of Herschel-Bulkley were increased by 5%. In analytical analysis the values of molecular viscosity and sensitivities of viscosities were calculated. In CFD analysis the sensitivities of rotor power, surface velocity and average velocity in the vat were defined.

6.3.1 Analytical results

For analytical sensitivity analysis the viscosity of Herschel-Bulkley model was plotted against shear rate. The values of experimental parameters are from the work of Mustalahti (2015, p. 58) with a suspension consistency of 4%. Viscosities were also determined for cases with 5% increased parameter values. These cases were also plotted in same figure. The results can be seen in Fig. 36. For shear rate the scale is logarithmic, since the extent of the range is large. In Fig. 36 the vertical dash lines illustrate the average shear rates in vat and moving reference frame in case 1. The critical shear rate of Herschel-Bulkley model is also plotted. The average shear rates in case 1 were used since it was used as a reference in CFD analysis. Changing Herschel-Bulkley model parameters changes effective viscosity quite little at high shear rate. The change is clearly bigger at low shear rate levels.

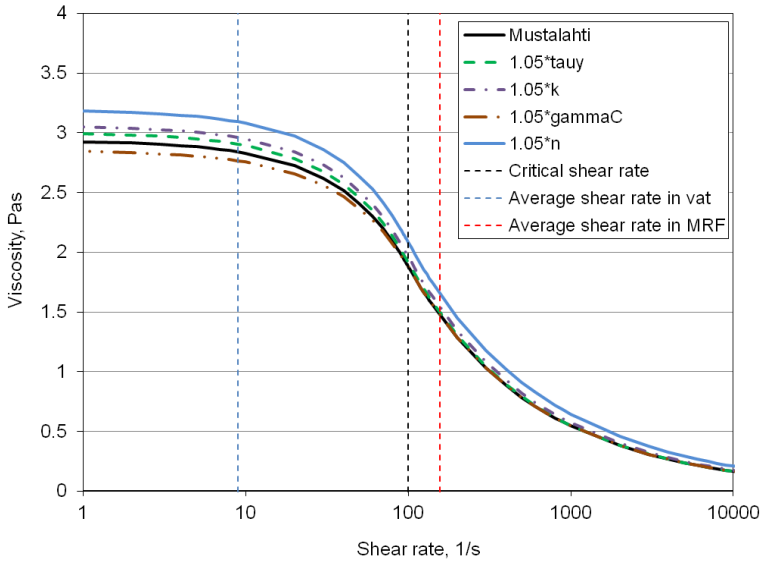

Figure 36. *The effect of change in experimental parameters on apparent viscosity in Herschel-Bulkley model.*

For sensitivity analysis the sensitivity of a function f in terms of variable x was defined as

$$S = \frac{\frac{\Delta f}{f}}{\frac{\Delta x}{x}}. \tag{6.1}$$

In Eq. 6.1, Δf is the change of function f when variable x is changed by Δx. For molecular viscosity calculations a representative shear rate had to be determined. The average strain rate in vat in case 1 was used. Apparent molecular viscosities were calculated as described in Eq. 2.13. The results of analytical sensitivity analysis are listed in Table 5.

Table 5. *The sensitivities of parameters in Herschel-Bulkley model.*

	μ_{ap}	S
Mustalahti	2.84	
$1.05 \times \tau_y$	2.86	0.15
$1.05 \times k$	2.96	0.85
$1.05 \times n$	3.09	1.78
$1.05 \times \dot{\gamma}_c$	2.77	-0.52

Increasing n, k and τ_y increases molecular viscosity. Viscosity decreases slightly when $\dot{\gamma}_c$ is increased. It is logical that n has the greatest sensitivity, since it is in the exponent of $\dot{\gamma}$. The results of analytical sensitivity analysis are logical and in line with the theory.

6.3.2 CFD analysis

The cases of 5 % increased Herschel-Bulkley parameter values were also simulated using CFD. The results of these cases are presented in Table 6. The results are presented relative to case 1. The only change between cases is in material parameters.

Table 6. *Results of CFD sensitivity analysis.*

	Case 14	Case 15	Case 16	Case 17
Increased variable	n	k	τ_y	$\dot{\gamma}_c$
Power	1.001	1.001	1.000	1.000
Power sensitivity	0.018	0.011	0.003	-0.005
Average surface velocity	0.955	0.985	0.999	0.999
Sensitivity of average surface velocity	-0.907	-0.292	-0.030	-0.021
Average velocity in vat	0.977	0.993	0.999	1.000
Sensitivity of average velocity in vat	-0.455	-0.145	-0.015	-0.007

Changing the material parameters had only a marginal effect on rotor power. The average velocity in vat and on the surface of vat in cases 16 and 17 are virtually the same as in case 1. In cases 15 and 16 the corresponding velocities drop. This is logical, since changing n or k increases molecular viscosity more than increasing τ_y. Surface velocity was clearly more sensitive to material model parameter modifications than average velocity in vat. This is logical, since the velocity on surface is created by momentum that has passed through the suspension.

7. CONCLUSIONS

The objective of this thesis project was to perform a thorough CFD analysis of a horizontal pulper. 17 different cases were simulated and analyzed. Simulations yielded extensive data of suspension flow in a pulper. Quantities describing mixing, flow rate and rotor efficiency were defined. Also three quantities were defined to describe pulping performance. These quantities were used to evaluate the performance of the pulper and different rotors.

Pulper performance analysis showed that in the base case configuration (cases 1 and 4) the whole vat was agitated and the pulper seemed to work as expected. Rotors 4 and 5 were more efficient and produced more effective pulping than rotor 1. Only high intensity turbulence generation was stronger with rotor 1. Due to this, also, turbulence dissipation rate isovolumes of rotors 4 and 5 at high threshold values were low. High pump blades in rotor 2 yielded slightly better efficiency, higher velocities in vat and better pulping performance than rotor 1. Wide blade tips in rotor 3 decreased rotor power, but flow rate, rotor efficiency and all pulping performance indicators also dropped. Based on the simulations it could be concluded that high pump blades and the geometry of rotor 4 would probably be good improvements to the pulper.

Sensitivity analysis was carried out to examine the effect of material model to simulation results. Herschel-Bulkley model parameters were increased by 5 % one at a time. The material model was studied analytically and using CFD. Analytical analysis of material model showed that molecular viscosity of Herschel-Bulkley model was the most sensitive respect to n and k. Changing these parameters affected also CFD results more than changing τ_y or $\dot{\gamma}_c$. Surface velocity was more sensitive to material model parameter changes than average velocity in the vat. Rotor power was really insensitive to material model parameter changes.

In this study measurements were not performed. No relevant measurement results were found in the literature either. Thus the results of this study could not be verified with measured data. Also uncertainties related to material model caused uncertainty to the results in pulper simulations. The strength of CFD in pulp suspension simulation laid on the ability to simulate multiple cases in a short time. Even if the results were not exact, the comparison of different simulations yielded reliable results. In this study comparison of different pulper setups was prioritized and thus CFD simulation was a good way to analyze the cases. As expected, increasing rotor rotational speed increased rotor power in simulations. Increasing suspension consistency decreased threshold integral volumes and average velocities in the vat. Also the changes in material model yielded credible results. These matters indicated that the results of this study were reliable.

In the literature study very few pulper performance analyses were found. This study provided a lot of new results in this field of research. However, it should be noted that the results cannot be entirely generalized. Pulper's performance depends significantly on rotor and vat geometries. More fundamental research would be needed to derive general correlations between rotor and vat geometry and pulper performance.

The lack of comprehensive publications related to pulper performance led to definition of six new criterion describing pulper performance. These parameters should be further reviewed and tested to establish their use in pulper design projects. In future the established pulper performance criteria make comparing different pulper setups easier. Also new performance criteria to evaluate defibering could be developed. Defibering criteria for simulation are particularly useful in pulper development. The Simulation results from this study would permit also further analysis of the pulper's performance, if new performance criteria arise. Experimental studies should be carried out to verify the results found in this study. However, it is really difficult, and often impossible, to conduct flow measurements in a pulper. Thus, simulation is often the only way to visualize flow in a pulper.

REFERENCES

ANSYS. (2015) Fluent User's Guide, ANSYS.

Arjas, A. (1983) Paperin valmistus, Suomen Paperi-insinöörien yhdistys r.y., 724 s.

Bennington, C. (1988) Mixing pulp suspensions, University of British Columbia, 323 p.

Bennington, C., & Kerekes, R. (1996) Power requirements for pulp suspension fluidization, Tappi Journal, Vol. 79, No. 2, pp. 253-258.

Bhole, M., Ford, C., Bennington, C.P.J. (2009) Characterization of axial flow impellers in pulp fibre suspensions, Chemical Engineering Research and Design, Vol. 87, pp. 648-653.

Boersma, W. H., Laven, J., Stein, H. N. (1992) Viscoelastic properties of concentrated shear-thickening dispersions, Journal of Colloid and Interface Science, Vol. 149, No. 1, pp. 10-22.

Chase, W.C., Donatelli, A.A., Walkinshaw, J.W., (1989) Effects of freeness and consistency on the viscosity of hardwood and softwood pulp suspensions, Tappi Journal, Vol. 72, No. 5, pp. 199-204.

Chhabra, R. P. (2008) Non-Newtonian Flow and Applied Rheology: Engineering Applications, Second Edition, Elsevier Ltd, 518 p.

Cotas, C., Asendrych, D., & Rasteiro, M. G. (2015) Numerical simulation of turbulent pulp flow of concentrated suspensions: influence of the non-newtonian properties of the pulp, Particulate Science and Technology, Vol. 34 No. 4 pp. 442-452.

Cotas, C., Asendrych, D., Garcia, F., Faia, P., & Rasteiro, M. G. (2015) CFD simulation of a turbulent fiber suspensionflow – a modified near-wall treatment, Engineering Applications of Computational Fluid Mechanics, pp. 233-246.

Demler, C., Egan, J. (2004) How To Reduce Pulper Operating Costs by Thirty Percent: Report on new rotor and bedplate technologies, Association Technique de L'Industrie Papetiere, Vol 58, No. 5, pp. 42-48.

Derakhshandeh, B. (2011) Rheology of Low to Medium Consistency Pulp Fibre Suspensions. Vancouver: The University of British Columbia, 127 p.

Derakhshandeh, B., Kerekes, R., Hatzikiriakos, S., & Bennington, C. (2011) Rheology of pulp fibre suspensions: A critical review, Chemical Engineering Science, Vol. 66, pp. 3460–3470.

Dickenson, C. (1988) Pumping Manual 8th Edition, The Trade & Technical Press Limited, 746 p.

Duffy G. G., The unique behaviour of wood fiber suspensions, Proceedings of the 9th International Conference on Transport and Sedimentation of Solid Particles, September, 1997.

Ein-Mozaffari, F., Bennington, C.P.J., Dumont, G.A. (2005) Suspension yield stress and the dynamic response of agitated pulp chests, Chemical Engineering Science, Vol. 60, No. 8-9, pp. 2399-2408.

Hammarström, D. (2004) A Model for Simulation of Fiber Suspension Flows, KTH Mechanics, Royal Institute of Technology, 95 p.

Hoffman, R. L. (1974) Discontinuous and dilatant viscosity behavior in concentrated suspensions. II. Theory and experimental tests, Journal of Colloid and Interface Science, Vol. 46, No. 3, pp. 491-506.

Huhtanen, J-P. (2004) Modeling of fiber suspension flows in refiner and other papermaking processes by combining non-Newtonian fluid dynamics and turbulence, Tamperer University of Technology, 110 p.

Hämäläinen, J., Lindström, S. B., Hämäläinen, T., & Niskanen, H. (2010) Papermaking fibre-suspension flow simulations at multiple scales, Journal of Engineering Mathematics, Vol. 71, pp. 55-79.

Jiulong Sha, A. N. (2015) The Effect of Consistency and Freeness on the Yield Stress of Chemical Pulp Fibre Suspensions. BioResources, Vol. 10, No. 3, pp. 4287-4299.

Jäsberg, A. (2007) Flow behaviour of fibre suspensions in straight pipes: new experimental techniques and multiphase modeling. Jyväskylä: University of Jyväskylä., 157 p.

Kerekes, R. J., Schell, C. J. (1992) Characterization of fibre flocculation by a crowding factor, Journal of Pulp and Paper Science, Vol. 18, No. 1, pp. 32-38.

Malvern, L. E. (1969) Introduction to the Mechanics of a Continuous Medium, New Jersey: Prentice-Hall Inc., 713 p.

Morrison, F. A. (2001) Understanding Rheology, Oxford University Press, 545 p.

Mustalahti, K. (2015) Vesikuitususpension virtausominaisuuksien mittaus, Tampereen teknillinen yliopisto, 74 s. Saatavissa: http://dspace.cc.tut.fi/dpub/bitstream/handle/123456789/22910/Mustalahti.pdf?sequence=1

Oliveira, P., Pinho, F. (1998) A qualitative assessment of the role of a viscosity depending on the third invariant of the rate-of-deformation tensor upon turbulent non-Newtonian flow, Journal of Non-Newtonian Fluid Mechanics, Vol. 78, pp. 1-25.

Olson, J. (2005) Pulp Suspensions, Lecture notes, University of British Columbia, 14 p. Available: http://www.fibrelab.ubc.ca/files/2013/01/Topic-4-Mechanical-Pulping-Pulp-Suspension.pdf

Paulapuro, H. (2008) Papermaking Part 1, Stock Preparation and Wed End, 2nd Edition, Finnish Paper Engineers' Association/Paperi ja Puu Oy, 516 p.

Pinho, F. (2003) A GNF framework for turbulent flow models of drag reducing fluids and proposal for a k–ε type closure, Journal of Non-Newtonian Fluid Mechanics, Vol. 114, pp. 149-184.

Robertson, A.A., Mason, S.G. (1957) The flow characteristics of dilute fibre suspensions, Tappi, Vol. 40, No. 50, pp. 326-335.

Savolainen, A., Jussila, T., Nikula, S. (1991) Defibering and specific energy consumption in bale pulpers. Tappi Journal, pp. 147-153.

Standard T 227 (1999) Freeness of pulp (Canadian standard method), Pulp Properties Committee of the Process and Product, TAPPI, 9 p.

Swerin, A., Powell, R.L., Odberg, L. (1992) Linear and nonlinear dynamic viscoelasticity of pulp fibre suspensions, Nordic Pulp Paper Research Journal Vol. 7, No. 3, pp. 126–143.

Valmet Technologies Inc. (2015) Operator and Mechanical Maintenance Training material for OptiSlush Broke, Valmet Technologies, 157 p.

Versteeg, H. K. (2007) An introduction to Computational Fluid Dynamics The Finite Volume Method, 2nd edition, Pearson Education Limited, 503 p.

Voith Paper. (2016) Voith deflaker product sheet, 2 p. Available: http://www.voith.com/en/667_Deflaker_vp_fs_1017_en_01-Screen.pdf

Wilcox, D. (1993) Turbulence Modeling for CFD, DCW Industries, 460 p

APPENDIX A: ADDITIONAL FIGURES

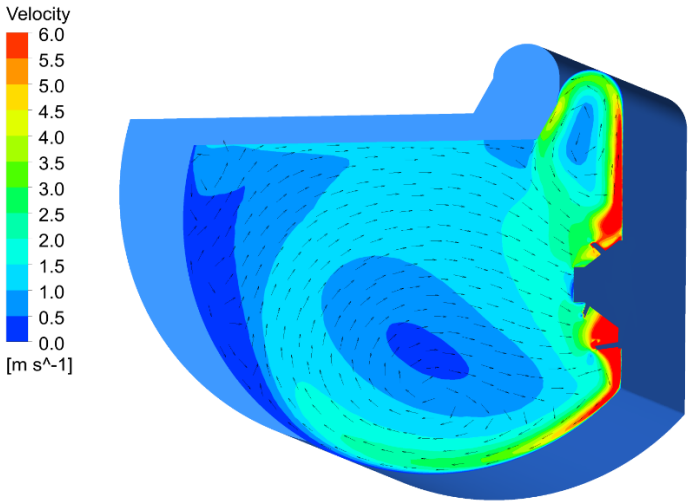

Figure A1. *Velocity contour in vat cross-section in case 12.*

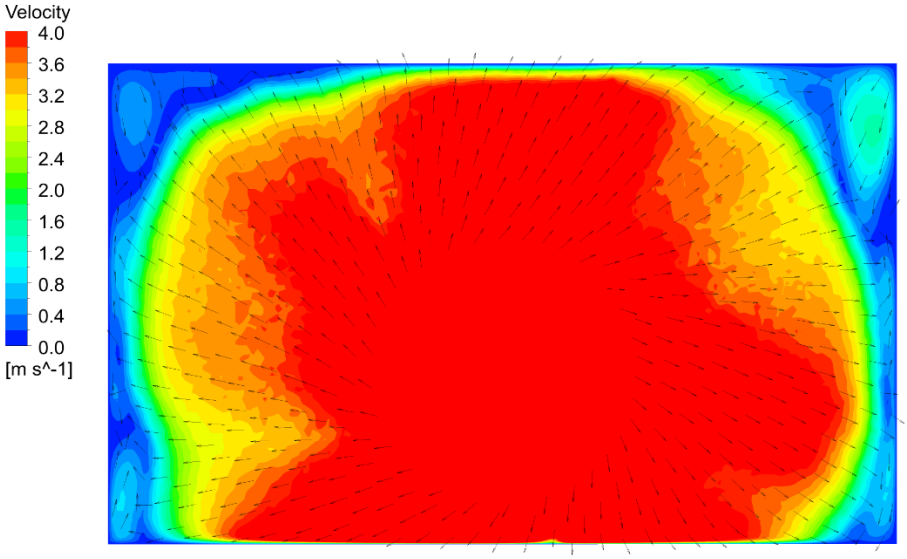

Figure A2. *Velocity contour 5 cm from back wall in case 12.*